Title

The Dupal isotopic anomaly in the southern Paleo-Asian Ocean: Nd–Pb isotope evidence from ophiolites in Northwest China

Authors

Liu, Xijun
Xu, Jifeng
Castillo, Paterno R
et al.

Publication Date

2014-02-01

DOI

10.1016/j.lithos.2013.08.020

Peer reviewed

Lithos 189 (2014) 185–200

Contents lists available at ScienceDirect

Lithos

journal homepage: www.elsevier.com/locate/lithos

The Dupal isotopic anomaly in the southern Paleo-Asian Ocean: Nd–Pb isotope evidence from ophiolites in Northwest China

Xijun Liu [a,b,c,d], Jifeng Xu [b,*], Paterno R. Castillo [c,**], Wenjiao Xiao [d], Yu Shi [a,e], Zuohai Feng [a], Lin Guo [a]

[a] Guangxi Key Laboratory of Hidden Metallic Ore Deposits Exploration, Guilin University of Technology, Guilin 541004, China
[b] Key Laboratory of Isotope Geochronology and Geochemistry, Guangzhou Institute of Geochemistry, CAS, Guangzhou 510640, China
[c] Scripps Institution of Oceanography, UCSD, La Jolla, CA 92093, USA
[d] Xinjiang Research Center for Mineral Resources, Xinjiang Institute of Ecology and Geography, Chinese Academy of Sciences, Urumqi 830011, China
[e] State Key Laboratory for Mineral Deposits Research, School of Earth Sciences and Engineering, Nanjing University, Nanjing 210093, China

ARTICLE INFO

Article history:
Received 27 February 2013
Accepted 27 August 2013
Available online 3 September 2013

Keywords:
Ophiolite
Paleo-Asian Ocean
Indian MORB-type mantle domain
Dupal anomaly

ABSTRACT

It has been suggested that the Dupal isotopic anomaly in the mantle can be traced in the Paleozoic ophiolites from the Neo- and Paleo-Tethyan Ocean (275–350 Ma). The Karamaili ophiolite (KO) and Dalabute ophiolite (DO) in the eastern and western corners, respectively, of the Junggar basin in NW China represent remnants of the relatively older (>350 Ma) Paleo-Asian Ocean (PAO) crust. Thus, these ophiolites can provide additional constraints on the long-term composition and evolution of the Paleozoic suboceanic mantle. We present new major-trace element and Sr, Nd and high-precision Pb isotope data for the basalts, gabbros and a plagioclase separate from the KO and DO. Our results indicate that the PAO crust indeed has a Dupal-like isotopic signature. In detail, all samples have relatively low $\varepsilon_{Nd(t)}$ and high $^{208}Pb/^{204}Pb_{(t)}$ for given $^{206}Pb/^{204}Pb_{(t)}$ ratios (i.e., positive $\Delta 8/4$ values), similar to the Dupal isotopic characteristics of Indian Ocean mid-ocean ridge basalts (MORB). The trace element signature of DO mafic rocks is similar to that of normal- and enriched-MORB whereas that of the KO is transitional between MORB and arc basalt. Therefore, the DO mantle domain reflects the PAO asthenosphere and the KO domain additionally shows the influence of the subduction process. Geochemical modeling using Th/Nd as well as Nd and Pb isotopic ratios indicates that up to 2% subduction component had been added to a depleted Indian MORB-type mantle to produce the bulk of KO rocks. The subduction component in the KO rocks consisted of variable proportions of ≤1% partial melt of unradiogenic sediment similar to modern Izu–Bonin trench sediment and hydrous fluid dehydrated from the subducted altered oceanic crust. The Devonian asthenospheric mantle beneath the southern PAO is isotopically heterogeneous, but lends support to the idea that the Dupal isotopic anomaly existed prior to the opening of the Indian Ocean. Finally, plate tectonic reconstruction indicates that the anomaly was present in the Neo- and Paleo-Tethyan oceans in the southern hemisphere and in the southern part of PAO in the northern hemisphere during the late Paleozoic.

1. Introduction

Mid-ocean ridge basalts (MORB) from the Indian Ocean are isotopically distinct from Pacific–North Atlantic MORB in that they have higher $^{208}Pb/^{204}Pb$, $^{207}Pb/^{204}Pb$, $^{87}Sr/^{86}Sr$ and lower $^{143}Nd/^{144}Nd$ for a given $^{206}Pb/^{204}Pb$ ratio (Dupre and Allegre, 1983; Hamelin and Allegre, 1985; Hart, 1984; Mahoney et al., 1992, 1998; Xu and Castillo, 2004; Xu et al., 2002). This isotopic signature of Indian MORB is typical of oceanic lavas with the so-called Dupal isotopic anomaly; these lavas are believed to originate from two large regions in the lower mantle with atypical isotopic and seismic velocity characteristics (Castillo, 1988; Hart, 1984). One possible explanation for the occurrence of Dupal lower mantle domains is that these were produced early in the Earth's history by core–mantle–crust differentiation processes (Castillo, 1988; Hart, 1984). Such a genesis requires that the domains are long-lived regional features of the mantle (Xu and Castillo, 2004; Xu et al., 2002). Thus, understanding the long-term history and evolution of the sub-Indian mantle may lead to a better understanding of the genesis of the compositional and structural heterogeneity of the lower mantle.

Ophiolites, which are pieces of ocean floor that are occasionally preserved on land (e.g., Dilek, 2003; Hawkins, 2003), are an important source of geologic information on the formation and subsequent closure of oceanic basins (Moores and Jackson, 1974; Shervais, 2001; Shervais et al., 2005). The trace element and isotopic characteristics of ophiolites generally reflect those of the composition and evolution of their underlying mantle (e.g., Mahoney et al., 1998; Pfänder et al., 2002; Xu and

* Correspondence to: J. Xu, Key Laboratory of Isotope Geochronology and Geochemistry, Guangzhou Institute of Geochemistry, Chinese Academy of Sciences, Guangzhou 510640, China. Tel.: +86 20 85290282.
** Correspondence to: P.R. Castillo, Scripps Institution of Oceanography, UCSD, Geosciences Research Division, La Jolla, CA 92093-0212, USA. Tel.: +1 858 534 0383.
E-mail addresses: xijunliu@gmail.com (X. Liu), jifengxu@gig.ac.cn (J. Xu), pcastillo@ucsd.edu (P.R. Castillo).

0024-4937/$ – see front matter © 2013 Elsevier B.V. All rights reserved.
http://dx.doi.org/10.1016/j.lithos.2013.08.020

Castillo, 2004; Xu et al., 2002; Zhang et al., 2005). For example, previous geochemical and isotopic studies of the late Paleozoic Neo- and Paleo-Tethyan ophiolites (Xu and Castillo, 2004; Xu et al., 2002; Zhang et al., 2005) showed that the bulk of Indian suboceanic mantle was most probably inherited from the Tethyan asthenosphere, which formerly occupied much of the present Indian Ocean region. Thus, these studies proposed that the Dupal isotopic anomaly existed prior to the opening of the Indian Ocean. However, what was the regional extent and how far back in time did the distinct mantle isotopic characteristics exist?

The extinct Tethys and Paleo-Asia Ocean (PAO) co-existed during the Paleozoic. Ophiolites representing relict fragments of the Tethyan and PAO crusts are preserved along the Tethys and PAO suture zones. The PAO is believed to have existed from ~1000 to ~300 Ma (Dobretsov et al., 1995; Dobretsov et al., 2003). It is slightly older than the late Paleozoic Neo- and Paleo-Tethyan Ocean (275–350 Ma; Xu and Castillo, 2004; Xu et al., 2002; Zhang et al., 2005). The Central Asian Orogenic Belts (CAOB), which is also known as the Altaid tectonic collage (Sengör and Natal'in, 1996; Sengör et al., 1993), is a subduction–accretionary complex associated with the evolution and closure of the PAO. The Karamaili ophiolite (KO) and Dalabute ophiolite (DO) are the two largest Devonian ophiolite belts in the Xinjiang region in northern China; these represent relict pieces of the crust of the southern branch of the PAO (W.J. Xiao et al., 2009) in the CAOB (Jahn, 2004). As in other typical ophiolites, most of the original rock sequences in the KO and DO are not preserved completely, but they have almost all the igneous components of a classic ophiolite (mantle peridotites, cumulate ultramafics, gabbros, and volcanics). Thus, the chemical variation of mafic rocks from the KO and DO can provide key information on the sub-PAO mantle and magma differentiation processes that formed these ophiolites. Systematic isotopic studies, especially involving combined Sr–Nb–Pb isotopes, on PAO ophiolites have not been carried out thus far.

The main objective of this paper is to constrain the geochemical and isotopic composition of the sub-PAO mantle in order to constrain the temporal and spatial extent of the Indian Ocean-type asthenospheric mantle. To attain this objective, we performed a comprehensive major-trace element and Sr, Nd and high-precision Pb isotopic investigation of KO and DO mafic rocks and combined these with existing major and trace element data (Liu et al., 2007, 2009b). Our main conclusion is that the PAO was indeed underlain by an Indian Ocean-type mantle domain as early as late Paleozoic, but caution must be taken because the subduction process had clearly modified the original composition of the mantle beneath the majority of ophiolites.

2. Geological background

The southern portion of CAOB is in the northern Xinjiang region of China (Fig. 1a). From north to south, it is composed of the Altaid Junggar and Tienshan terranes. The Junggar terrane is traditionally further subdivided into East Junggar and West Junggar terranes and Junggar basin. The East and West Junggar are two accretionary terranes located to the east and west of Junggar basin, respectively, and thought to be the result of northward subduction of the Paleozoic PAO crust beneath the Siberian Plate (Coleman, 1989; Sengör et al., 1993; W.J. Xiao et al., 2009; Xiao et al., 2004a, 2004b; Zhang et al., 2009).

2.1. Karamaili ophiolite (KO)

The KO is one of the two partial and dismembered ophiolite sequences in the southern part of East Junggar; the other is the Armantai ophiolite in the central part of East Junggar (Fig. 1a). Associated with these ophiolites are two remnant arcs, the Dulate–Baytag arc in the northern side of Armantai ophiolite and the Yemaquan arc in the northern side of KO. The KO is part of a forearc accretionary complex (W.J. Xiao et al., 2009), which is similar to modern circum-Pacific forearc accretionary belts in that it contains sedimentary and volcanic rocks, ophiolitic fragments that include extrusive sequences, plutonic complex and upper mantle units, and the bulk of its accretionary prism is variably metamorphosed to greenschist facies. The overall structural geometry, abundance and types of the rock suites present, petrogenetic relationships between rock suites, and variations of deformation and metamorphism strongly resemble those of the Japan island arc orogens (W.J. Xiao et al., 2009).

In detail, the KO forms a NWW-trending belt and crops out mainly along the Karamaili fault for about 150 km (Fig. 1a). It extends from Kamste in the northwest and continues southeastwards through the Moqinwula Mountains, farther east through the China–Mongolia border, and finally to the Zoolen ophiolite belt in Mongolia (Helo et al., 2006). The western extension of the KO belt is covered by Cenozoic sediments in the Junggar basin (Li et al., 2003). There are two types of outcrops in the KO belt: ophiolite sequences and associated series of volcanic rock units. Although the entire KO belt is dismembered, individual fragments of relatively intact ophiolite sequences are present. These fragments consist of large volumes of serpentinized peridotites, serpentinites, and cumulate pyroxenites; these upper mantle units, are overlain by plutonic complexes including gabbros, diabases, sparse sheeted dikes and felsic plutons, and, finally, upper extrusive sequences including basalts, red cherts and green siliceous mudstones containing Devonian and Carboniferous radiolaria (Cai, 1986; He et al., 2000; Shu and Wang, 2003). The ultramafic rocks occur as pods and lenses and are strongly serpentinized although they still contain relict olivine and pyroxene. Serpentinites are mainly metamorphosed harzburgite, dunite and minor lherzolite, and host minor pods of chromitites. The mafic rocks mainly occur as tectonic slices containing cumulate and isotropic gabbros. There are also some associated, purportedly younger volcanic rock units and these consist mainly of massive basalt flows and some pillows.

Previous reconnaissance studies indicated that the mafic rocks (gabbros and basalts) in the KO are mainly transitional in composition between MORB-like to island arc tholeiite (IAT)-like (Liu et al., 2007, 2009b); others have also reported basalts with enriched-MORB, ocean island basalt (OIB) and boninite characteristics (Bu et al., 2005; Ma, 2007; Ouyang, 2006; Zheng et al., 2007). There are also silicic rocks associated with the KO. Most of these intruded the mafic rocks and include many variably shaped bodies of interlayered diorites, quartz–diorites, tonalites, and plagiogranites in the northern side of the ophiolite (Fig. 1a). Some plagiogranite bodies intersect the gabbros discordantly or display direct contact relationship suggesting contemporaneity. The rest of the intermediate-silicic rocks consist of andesites and dacites. The age of KO has been determined by U–Pb zircon dating, and includes 336 Ma and 342 Ma for the gabbros (Jian et al., 2005), 403 Ma (Jian et al., 2005) and 373 Ma (Tang et al., 2007) for the plagiogranites and 371 Ma for the tonalites (Liu et al., 2009b). These age data indicate that our samples of the KO crust range in age from 371 Ma to 403 Ma; these are consistent with the Devonian and Early Carboniferous age of the radiolarian cherts (Cai, 1986; He et al., 2000; Shu and Wang, 2003). Finally, although the KO was definitely formed in a subduction environment, the details of its formation are still in dispute. Some argue that the KO was formed in a back-arc basin (Li, 1995; Li et al., 2003; Ma, 2007) or in a forearc region

Fig. 1. Geological sketch map of a) the East Junggar region and b) the west Junggar region. Inset is a simplified tectonic map of central Asia (after Jahn, 2004) and Northern Xinjiang (after Xiao et al., 2008; W. Xiao et al., 2009) showing the distribution of ophiolites. The Central Asian Orogenic Belt (CAOB) is located between Siberian craton in the north and Tarim-North China craton in the south. The northern Xinjiang region of China is composed from north to south of the Altaid, Junggar and Tienshan terranes. The ophiolite belts are mainly distributed around Junggar basin. The approximate location of the northern Xinjiang region of China is indicated.
Panel A is modified after Li et al. (2003) and W.J. Xiao et al. (2009). Panel B is modified after Liu et al. (2009c) and Lei et al. (2008).

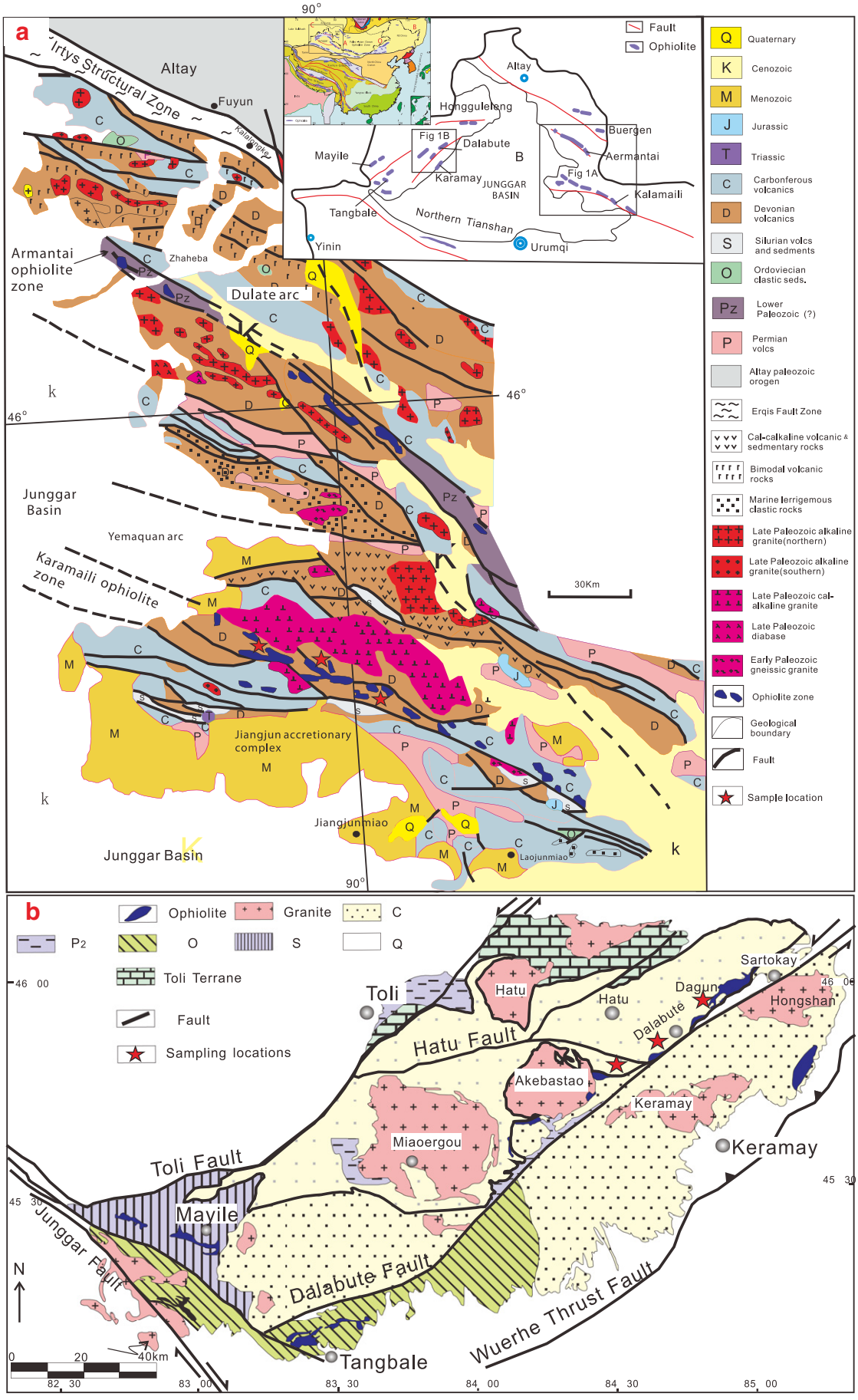
a
Irtys Structural Zone
Altay
Fuyun
Katalighka
Armantai ophiolite zone
Zhaheba
Dulate arc
Junggar Basin
Yemaquan arc
Karamaili ophiolite zone
Jiangjun accretionary complex
Jiangjunmiao
Laojunmiao
Junggar Basin
90°
46°
30Km
Fault
Ophiolite
Hongguleleng
Fig 1B
Dalabute
Mayile
B
Karamay
JUNGGAR BASIN
Fig 1A
Buergen
Aermantai
Kalamaili
Tangbale
Northern Tianshan
Yinin
Urumqi
Q Quaternary
K Cenozoic
M Menozoic
J Jurassic
T Triassic
C Carbonferous volcanics
D Devonian volcanics
S Silurian volcs and sedments
O Ordovician clastic seds.
Pz Lower Paleozoic (?)
P Permian volcs
Altay paleozoic orogen
Erqis Fault Zone
Cal-calkaline volcanic & sedmentary rocks
Bimodal volcanic rocks
Marine terrigemous clastic rocks
Late Paleozoic alkaline granite(northern)
Late Paleozoic alkaline granite(southern)
Late Paleozoic cal-alkaline granite
Late Paleozoic diabase
Early Paleozoic gneissic granite
Ophiolite zone
Geological boundary
Fault
Sample location
b
Ophiolite
Granite
C
P2
O
S
Q
Toli Terrane
Fault
Sampling locations
46 00
45 30
Toli
Hatu
Hatu
Sartokay
Dagun
Hongshan
Dalabute
Hatu Fault
Akebastao
Keramay
Miaoergou
Keramay
Toli Fault
Mayile
Junggar Fault
Dalabute Fault
Wuerhe Thrust Fault
Tangbale
N
0 20 40km
82 30
83 00
83 30
84 00
84 30
85 00

(Wang et al., 2003; Xiao et al., 2004a, 2004b), but more recently it was suggested to be a section of an arc setting that experienced ridge subduction (Liu et al., 2007, 2009b).

2.2. Dalabute ophiolite (DO)

The DO is one of the largest of the partial and dismembered ophiolite sequences in west Junggar (Fig. 1b). The DO forms a NE–SW-trending belt and crops out mainly along the Dalabute fault for about 100 km. It extends from Miaoergou in the southwest and continues southeastwards through the Dagun, an outcrop covering an area of ~50 km^2. The DO consists of tectonic slices that are mainly distributed in three locations along the Dalabute fault: Akebastao in the south, Dalabute in the middle, and Dagun in the north. Among these locations, the longest exposure of the ophiolite belt is in Dalabute, where it consists of at least 9 mafic and ultramafic outcrops. Similar to the KO, the entire ophiolite igneous sequences ranging from bottom ultramafic units to top mafic units are present. These include large volumes of serpentinized peridotites, serpentinites, cumulates, sparse diabases, sheeted dikes, and upper extrusive sequence of basalts. Above the igneous sequence are red cherts that also contain Devonian radiolarian (Xiao et al., 1992).

Previous studies indicated that the bulk composition of DO mafic rocks (gabbros and basalts) is akin to normal- and enriched-MORB and OIB (Liu et al., 2009c; Zhang et al., 2011). The DO age has been reported by many studies, and includes a Sm–Nd isochron age of 395 Ma for the gabbros (Zhang and Huang, 1992) and more recent U–Pb zircon ages of 391 Ma (Gu et al., 2009) and 332 Ma (Xu et al., 2006) for the gabbros. Another previous study reported a 302 Ma age for a gabbro, but this belongs to a later suite of mafic rocks (Liu et al., 2009c). Although quite variable, these igneous ages of the ophiolite combined with the Devonian age of the radiolarian cherts (Xiao et al., 1992) give a conclusive Early Devonian age (391–332 Ma) of the DO, although as noted earlier some younger magmas related to the ophiolite are also present.

3. Petrography

The igneous rocks from the different sections of KO and DO have distinctive petrographic characteristics, but in general there is no petrographic difference between KO and DO rock suites. Both whole rock sequences had been affected by oceanic hydrothermal alteration and subjected to sub-greenschist facies condition; thus, the extent of alteration is variable. Basalts, the most abundant rock in both volcanic suites, are black to gray greenish in outcrops. They are vesicular in the massive flows, amygdaloidal in the pillows, and predominantly aphyric to microphyric with equigranular to intergranular groundmass consisting of plagioclase, pyroxene and minor anhedral titanomagnetite. Plagioclase feldspars occur as euhedral to subhedral columnar laths that are 0.03 mm to 1 mm in length. Many samples contain euhedral plagioclase with little or no alteration, but some samples contain secondary mineral replacements along the edges of grains or along twin planes within crystals; other samples experienced serious alteration and showed replacement of the plagioclase by albite, zeolite and prehnite. Pyroxenes range in size from 0.05 mm to 1 mm and are generally unzoned and variably altered to chlorite, magnetite, actinolite, and epidote.

Plutonic rocks in both ophiolites are mainly gabbros. In outcrops gabbros are massive and dark gray in color and in thin sections they are coarse- to fine-grained, isotropic and contain variable amounts of olivine, pyroxenes, plagioclase feldspar, amphibole, and titanomagnetite. The gabbros are variably altered. Some of the olivines are pseudomorphed by chlorite and clay. Pyroxenes and plagioclase are only slightly altered and are the most abundant phases in the gabbros with modes ranging from 60% to 70%.

4. Analytical techniques

The mafic rocks analyzed include fine-grained gabbros, diabases and basalts. Prior to analysis, rock samples were crushed into small chips, highly altered chips and secondary vein materials were removed using a hand lens, and then the remaining chips were soaked in 4 N hydrochloric acid for half an hour in order to leach out alteration minerals. The rock chips were then powdered using an alumina ceramic shatterbox. Major elements were determined by X-ray fluorescence (XRF) method whereas trace element concentrations were measured using a PE Elan 6000 inductively-coupled plasma mass spectrometer (ICPMS) at the Guangzhou Institute of Geochemistry (GIG), Chinese Academy of Sciences. The analytical procedure for the ICP-MS analysis is similar to that described by Li (1997) and Chen et al. (2012). Trace element concentrations were drift corrected using the USGS standard sample BCR-1. Analytical uncertainties are generally less than 5–10%, depending upon concentrations.

Strontium and Nd isotopic compositions were measured using a Micromass Isoprobe multicollector mass spectrometer (MC-ICPMS) also at the GIG. Analytical procedures used are similar to those described by Wei et al. (2002), Liang et al. (2003) and Chen et al. (2012). Measured $^{87}Sr/^{86}Sr$ were corrected to mass fractionation using $^{86}Sr/^{88}Sr = 0.1194$. Strontium standard NBS987 was used to monitor instrumental performance and yielded an average $^{87}Sr/^{86}Sr$ ratio of 0.710242 ± 17 (2σ; n = 55). The measured $^{146}Nd/^{144}Nd$ and fractionation-corrected $^{143}Nd/^{144}Nd$ ratios of the JNdi-1 standard were 0.710288 ± 28 (2σ; n = 40) and 0.512109 ± 12 (2σ; n = 40), respectively. All measured Nd isotopic ratios were normalized to $^{146}Nd/^{144}Nd = 0.71029$. Uranium, Th and Pb elemental concentrations were measured on the same powder aliquots measured for Pb isotopes at the Scripps Institution of Oceanography (SIO), University of California, San Diego. The U, Th and Pb elemental concentrations were measured using a Finnigan Element 2 high-resolution inductively-coupled plasma mass spectrometer (HR-ICPMS) using the procedure described in Tian et al. (2008). Samples analyzed for Pb isotopic compositions were not leached because previous studies have shown that the differences in age-corrected Pb isotope ratios for leached–unleached pairs of old variably altered rocks are relatively small (Mahoney et al., 2002). Lead isotopic ratios were measured on a Micromass Sector 54 multicollector thermal ionization mass spectrometry (TIMS) also at SIO in a multicollector static mode using a ^{207}Pb–^{204}Pb double spike. The sample preparation procedure is also similar to that described in Tian et al. (2008) and has total blank of <100 pg Pb. The Pb isotopic compositions of each sample were measured twice as spiked and unspiked aliquots, the analytical and fractionation corrected following the procedure described in Liu and Liao (2012) and Liu et al. (2013) and adjusted to the Pb standard NBS981 values of Todt et al. (1996). The precision of Pb data is taken to be <0.03% per mass unit for $^{206}Pb/^{204}Pb$ and $^{207}Pb/^{204}Pb$ and <0.05% for $^{208}Pb/^{204}Pb$.

5. Results

5.1. Major and trace element

Almost all the mafic volcanic and intrusive rocks from the KO (Liu et al., 2009b) and DO that we analyzed are tholeiitic basalts (or gabbros) and basaltic–andesites (Fig. 2 and Table 1). These rocks are characterized by high Al_2O_3 and $Fe_2O_3^{total}$ and variable MgO and Mg# (molar Mg / [Mg + Fe^{2+}] * 100). The KO mafics have low (average <1 wt.%) TiO_2, similar to primitive normal-MORB (~0.6–1 wt.% TiO_2; Presnall and Hoover, 1987) or typical island arc basalts (<1 wt.% TiO_2; Thirlwall et al., 1994; Woodhead et al., 1993), whereas DO mafic rocks show slightly higher (average >1 wt.%) TiO_2, akin to enriched-MORB.

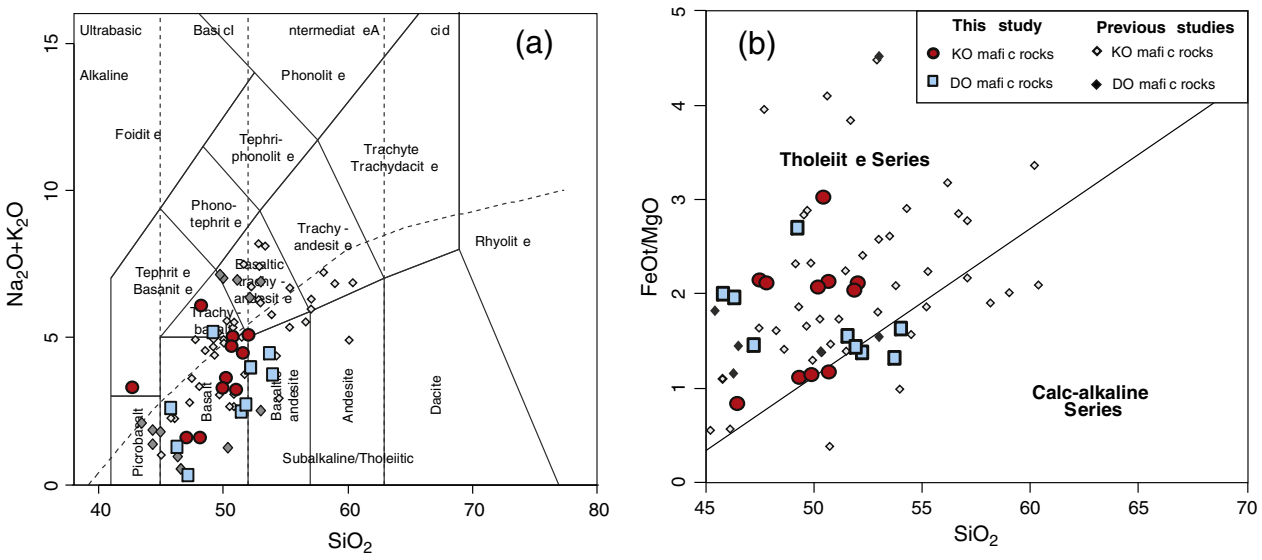

Fig. 2. Classification diagrams for KO and DO igneous rocks: (a) total alkali-silica (TAS) diagram after Le Bas et al. (1986), (b) FeOT/MgO vs SiO_2 after Miyashiro (1974). Shown for comparison are published data for KO mafic rocks (Liu et al., 2009b) and DO mafic rocks (Bu et al., 2005; Lei et al., 2008; Li, 1995; Ma, 2007; Ouyang, 2006; Wang et al., 2003; Zhang et al., 2009; Zheng et al., 2007).

The KO and DO mafic rocks display distinctive trace element characteristics. Although the KO mafic samples show a wide range of trace element concentrations, they can be subdivided into two distinct groups (Fig. 3). Group 1 is characterized by a light-REE depleted ($La/Sm_N = 0.51–0.88$) pattern similar to that of normal-MORB. However, it differs from normal-MORB in that it has distinctive negative HFSE anomalies. Such HFSE depletion is a characteristic feature of convergent margin lavas (e.g., Pearce and Peate, 1995; Pearce et al., 1984; Tatsumi and Kogiso, 2003). The only exception to the group is samples KL-24 and KL-27, which display normal-MORB like concentration patterns. On the other hand, Group 2 shows slight enrichment in light-REE ($La/Sm_N = 1.27–2.34$) similar to enriched-MORB. It also shows distinctive negative HFSE anomalies like Group 1.

The DO mafic rocks are characterized by a light-REE depleted to slightly enriched concentration pattern ($La/Yb_N = 0.55–2.26$) similar to that of normal-MORB to enriched-MORB. Their incompatible trace element patterns are also similar to that of normal- to enriched-MORB. In contrast to KO mafic samples, they do not have negative HFSE anomalies. Some KO and DO samples, however, have large positive Sr anomalies, perhaps related to seawater alteration.

In summary, DO mafic rocks from the western Junggar have a normal- to enriched-MORB trace element signature whereas KO mafic rocks from the eastern Junggar have transitional between MORB- and arc basalt-like signature. Therefore, in terms of trace elements, the DO mafic rocks came from a typical MORB mantle source and were most likely produced by seafloor spreading in an open ocean or mature back arc basin whereas KO mafic rocks may have come from a mantle source similar to that beneath the DO, but was additionally influenced by a relatively recent subduction process.

5.2. Sr–Nd–Pb isotope characteristics

Twenty one whole rock mafic samples from the KO and DO were analyzed for Sr, Nd and Pb isotopes, and one DO plagioclase separate for Pb isotopes. One should note that the Sr and Nd isotopes of eleven KO mafic samples were previously reported (Liu et al., 2009b). The isotopic analyses and their U, Th and Pb elemental abundances are presented in Table 2. Co-variations of their initial Sr and Nd isotope ratios at a crystallization age of 371 Ma (Liu et al., 2009b) are shown in Figs. 4 and 5. The $\varepsilon_{Nd(t)}$ values of KO and DO mafic samples fall completely within the range of age-corrected Pacific and Indian MORB fields. The $\varepsilon_{Nd(t)}$ values of the KO samples overlap although Group 1 mafic rocks extend to higher values (up to +9.7) whereas Group 2 mafic rocks extend to lower values (down to +6.2). Most DO samples display relatively lower $\varepsilon_{Nd(t)}$ values than KO samples and, thus, are more akin to Indian MORB values.

The initial Sr ratios $^{87}Sr/^{86}Sr_{(t)}$ of all mafic samples trend toward higher values (up to 0.7063) and, thus, are more radiogenic for given $\varepsilon_{Nd(t)}$ values relative to typical MORB. They all plot toward convergent margin arc lavas or seawater alteration. Therefore, the Sr isotopic ratios collectively are not considered a primary magmatic signature for these rocks.

The age-corrected Pb isotope compositions of KO and DO mafic samples are variable; for ease of comparison, all samples were also corrected to 371 Ma by using high-precision Th, U and Pb concentrations determined by HR-ICP-MS. In detail, the Pb isotopic ratios of KO and DO mafic rocks greatly overlap. However, several KO samples plot with age-corrected (to 371 Ma) Pacific MORB, but none of DO samples does (Fig. 5). Moreover, although there is no distinction between Group 1 and 2 KO samples, they have less radiogenic $^{207}Pb/^{204}Pb_{(t)}$ and $^{208}Pb/^{204}Pb_{(t)}$ for given $^{206}Pb/^{204}Pb_{(t)}$ ratios than DO mafic rocks. Combined with Nd isotopes, the Pb isotopic ratios additionally suggest a bi-modal distribution of KO and DO samples. All KO samples and two DO samples have relatively high $\varepsilon_{Nd(t)}$ for given low $^{206}Pb/^{204}Pb_{(t)}$ ratios whereas DO samples, except for the two above, have relatively lower $\varepsilon_{Nd(t)}$. The former group is similar to some Tethyan samples from the Shuangou and Mianlue ophiolites (Xu and Castillo, 2004; Xu et al., 2002) whereas the latter is akin to some Tethyan samples from the Jinshajiang ophiolite (Xu and Castillo, 2004). Significantly, these Nd and Pb isotopic features of the Tethyan and PAO ophiolites are also shown by the low $^{206}Pb/^{204}Pb$ Indian MORB (e.g., Mahoney et al., 1998, 2002).

In general, almost all KO and DO mafic samples plot above the northern hemisphere reference line (NHRL), or have high $^{207}Pb/^{204}Pb_{(t)}$ and $^{208}Pb/^{204}Pb_{(t)}$ for given $^{206}Pb/^{204}Pb$ ratios (i.e., positive Δ7/4 and Δ8/4 values), similar to age-corrected Indian MORB with a Dupal isotopic anomaly (Dupre and Allegre, 1983; Hart, 1984). They also plot within the fields for the 275–350 Ma Paleo-Tethyan MORB-like ophiolite lavas (Xu and Castillo, 2004; Xu et al., 2002; Zhang et al., 2005) and basalts from the Junggar basin, which had been interpreted as fragments of Paleozoic (395 to 405 Ma) PAO

Table 1
Major and trace element compositions of DO rocks.

Sample	DL-137	DL-139	DL-144	DL-145	DL-150	DL-153	DL-158	DL-159	DL-161
Rock type	Gabbro	Basalt	Gabbro	Gabbro	Basalt	Basalt	Basalt	Basalt	Basalt
Major elements (wt.%)									
SiO_2	51.52	45.74	46.34	46.73	51.55	49.05	46.11	50.32	50.32
TiO_2	1.25	1.6	0.82	1.36	1.09	1.15	1.24	1.18	1.08
Al_2O_3	17.99	13.75	12.50	7.99	14.53	14.67	16.51	15.49	14.24
$Fe_2O_3^{total}$	8.66	14.18	17.26	11.94	12.57	13.44	14.08	10.47	11.99
MnO	0.14	0.22	0.27	0.11	0.16	0.20	0.46	0.15	0.17
MgO	5.73	6.44	7.97	7.46	7.04	7.84	4.72	7.24	7.65
CaO	9.44	15.2	13.49	22.91	4.83	6.41	5.53	4.55	8.79
Na_2O	3.12	2.03	0.81	0.27	2.51	2.28	2.50	2.93	1.91
K_2O	0.8	0.53	0.45	0.00	1.06	0.05	2.36	1.26	0.72
P_2O_5	0.02	0.12	0.02	0.14	0.06	0.08	0.07	0.07	0.07
LOI	0.92	0.65	0.36	1.50	4.36	4.48	6.84	6.69	2.81
Total	99.6	100.45	100.29	100.41	99.74	99.66	100.43	100.34	99.74
Trace element (ppm)									
Sc	28.2	43.3	54.1	54.8	41.2	52.1	47.0	48.2	0.1
Ti	8278	10157	4994	8800	6242	7005	6895	7244	6256
V	208.6	320.4	394.4	478.8	314.2	337.9	323.7	258.9	300.6
Cr	209.7	197	51.54	12.21	152.7	150.2	161.8	107.2	157.4
Mn	1152	1742	2173	913.5	1160	1523	1620	1137	1286
Co	28.9	45.8	62.5	88.5	48.2	50.4	62.0	50.1	63.6
Ni	21.2	83.8	78.1	230.4	86.7	91.8	101.1	92.8	90.7
Cu	22.1	17.3	5.37	4.10	153.3	155.4	487.7	32.1	159.7
Zn	71.3	121.3	143.2	42.1	89.1	102.1	98.6	98.4	86.7
Sr	448.5	550.5	569.3	172.3	84.95	488.6	263.9	109	212.5
Rb	13.13	3.10	3.33	0.15	34.52	1.15	28.34	34.12	4.45
Y	17.76	28.35	22.22	24.47	19.07	23.33	19.58	19.62	8.05
Zr	84.93	117.7	32.66	52.57	50.59	60.39	56.56	57.57	53.74
Nb	3.55	6.64	3.02	1.30	2.43	2.82	2.59	2.78	2.58
La	5.76	6.46	1.77	3.02	2.96	3.45	3.19	3.45	2.30
Ce	14.56	17.23	4.79	8.00	7.83	8.98	8.61	8.96	7.61
Pr	2.26	2.72	0.81	1.30	1.27	1.45	1.46	1.46	1.15
Nd	10.37	12.37	4.21	6.76	6.39	7.07	7.12	7.22	5.50
Sm	2.78	3.67	1.59	2.48	2.14	2.31	2.36	2.37	1.79
Eu	1.23	1.25	0.62	1.25	0.84	0.89	0.96	0.94	0.70
Gd	3.17	4.42	2.42	3.39	2.93	3.00	3.26	3.07	2.23
Tb	0.55	0.80	0.50	0.71	0.59	0.58	0.63	0.62	0.44
Dy	3.40	4.94	3.37	4.56	3.87	3.57	3.99	3.85	2.78
Ho	0.71	1.04	0.81	1.01	0.81	0.79	0.85	0.85	0.60
Er	1.97	2.88	2.26	2.82	2.25	2.24	2.42	2.31	1.63
Tm	0.28	0.40	0.35	0.41	0.33	0.31	0.34	0.34	0.24
Yb	1.83	2.63	2.32	2.77	2.14	2.10	2.18	2.17	1.50
Lu	0.29	0.40	0.38	0.44	0.31	0.31	0.33	0.33	0.22
Hf	2.11	2.67	0.86	1.73	1.50	1.42	1.66	1.67	1.26
Ta	0.25	0.44	0.17	0.07	0.18	0.18	0.20	0.20	0.15
Th	0.94	0.50	0.09	0.17	0.27	0.26	0.29	0.29	0.01

LOI = loss on ignition. Mg# = 100 Mg / (Mg + Fe^{2+}) assuming Fe_2O_3 / FeO = 0.15.
Major element analyzed by XRF at the Guangzhou Institute of Geochemistry (GIG), Chinese Academy of Sciences. Trace element concentration are measured by ICP-MS also at GIG, the analytical uncertainties are generally less than 5–10%, depending upon concentrations.

crust (Zheng et al., 2007). Junggar basin samples on average, however, have lower $^{207}Pb/^{204}Pb_{(t)}$ but higher $^{208}Pb/^{204}Pb_{(t)}$ for given $^{206}Pb/^{204}Pb_{(t)}$ than KO and DO mafic samples.

6. Discussion

6.1. Mantle source composition

6.1.1. Trace element constraints

Ratios of incompatible trace elements, especially those with similar incompatibilities with respect to mantle rocks, have been used to constrain mantle sources (Condie, 2003). Almost all of our KO mafic rocks display HFSE/LILE depletion and LILE/REE enrichment. Specifically, many samples display slight Th enrichment relative to La as well as Nb depletion relative to Th compared to normal-MORB (Fig. 6a). Combined with previous results, however, KO igneous rocks display a wide range of Th/La and Nb/Th ratios, overlapping with the complete spectrum of magmas from forearcs to ocean ridges and oceanic islands. Such chemical variations indicate that the KO actually consists of both subduction-related as well as other oceanic igneous rocks. In other words, the bulk of our KO samples have the trace element signature of lavas derived from a depleted mantle source (or sources) contaminated by subduction-derived fluid(s) or mixing of magmas from a depleted mantle and recycled crustal materials (e.g., Condie, 2003; Godard et al., 2003, 2006; Peate and Pearce, 1998).

In comparison, the composition of DO mafic samples is similar to those of modern MORB and mature backarc basin basalts. Their HFSE/LILE and LILE/REE ratios are close to 1; together with previous results, these indicate that the source of DO mafic rocks is most likely a depleted, but slightly heterogeneous asthenospheric mantle.

The difference in the trace element composition of the mantle sources of KO and DO samples can be analyzed further using Th/Yb and Ta/Yb ratios (Fig. 6b). These ratios are excellent tracers of mantle source composition because they are largely independent of variations caused by degree of partial melting and crystal fractionation (Pearce and Peate, 1995). The element Th in marine sediments is more than 2 orders of magnitude larger than in the mantle (Plank and Langmuir, 1998) and highly soluble in melts but insoluble in fluids

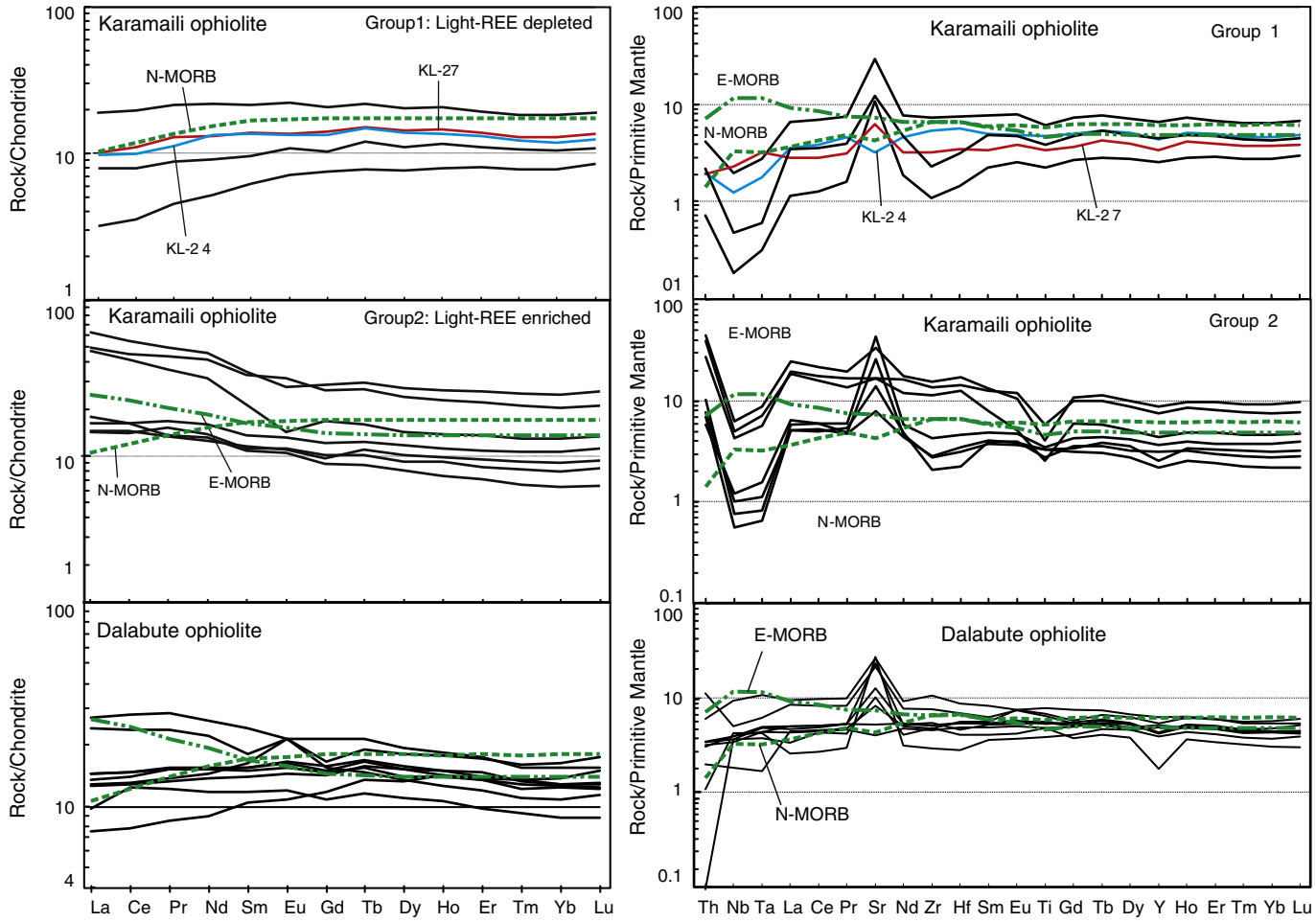

Fig. 3. Chondrite-normalized rare earth element (REE) concentrations and primitive mantle-normalized incompatible element concentrations of KO and DO mafic rocks. Chondrite and primitive mantle values are from Sun and McDonough (1989). The KO mafic rocks can be subdivided into two groups according to light-REE depleted ($La/Sm_N < 1$) and enriched ($La/Sm_N > 1$) concentration patterns. Values of N-MORB and E-MORB used are from Sun and McDonough (1989).

(Turner and Hawkesworth, 1997), Ta and Yb, unlike Th, are not enrichment in marine sediments and less effectively transferred from subducting slab to melting column (Pearce and Peate, 1995). Thus, Ta/Yb represents the degree of mantle enrichment or depletion of the mantle source (Pearce and Peate, 1995) whereas increasing Th/Yb ratio represents increasing sediment melt contribution (Class et al., 2000; Elliott et al., 1997; Singer et al., 2007). In other words, addition of sediment melt would result in addition of Th, but not Ta, to the mantle source and would make a vertical vector in Fig. 6b.

The KO igneous rocks have wide ranges of Th/Yb and Ta/Yb ratios, but most of them have higher Th/Yb for given Ta/Yb than MORB. Such relatively high Th/Yb ratios, plotting above the mantle array, indicate addition of melt from subducted sediment. In comparison, the bulk of DO samples show relatively low Th/Yb for given Ta/Yb ratios. Combined with published data, DO samples plot within the depleted- to enriched-MORB mantle array, suggesting a depleted to slightly enriched mantle source. Therefore, as above, the DO mafic rocks most likely originated from a slightly heterogeneous asthenospheric mantle whereas the mantle source of KO is more heterogeneous as it has the signature of a depleted mantle source that had been contaminated by subduction component.

6.1.2. Sr–Nd–Pb isotope constraints

Strontium is a fluid mobile element and is relatively abundant (8 ppm) in seawater. The exchange of Sr between rock and seawater during hydrothermal alteration of the oceanic crust raises the $^{87}Sr/^{86}Sr$ ratios of altered submarine rocks (e.g., Godard et al., 2006; Kawahata et al., 2001; McCulloch et al., 1981). Thus, the high $^{87}Sr/^{86}Sr_{(t)}$ ratios of KO and DO rocks are most likely due to seawater alteration and do not represent the primary magmatic composition of these rocks. In contrast, Nd is relatively immobile in fluid and the Nd isotopic values of altered submarine rocks remain unaffected until after the water/rock ratio reaches 10^5 (Faure and Mensing, 2004; McCulloch et al., 1981). Another source of concern is the mobility of U (when oxidized to U^{+VI}) and Pb during hydrothermal alteration as hydrothermal activity can significantly affect the Pb isotope systematics, especially in old samples (Faure and Mensing, 2004; Hauff et al., 2003). Consequently, we analyzed the Pb isotopic composition of the whole rock sample (DL-137) and its plagioclase separate (DL-137-pl) to see the extent of alteration in the Pb isotopes. Results show that their modern day Pb isotopic ratios are different, owing to differences in the respective parent (U, Th) and daughter (Pb) concentrations (Table 2). However, the age-corrected Pb isotopic values for the plagioclase ($^{206}Pb/^{204}Pb_{(t)} = 17.945$, $^{207}Pb/^{204}Pb_{(t)} = 15.533$ and $^{208}Pb/^{204}Pb_{(t)} = 37.994$) are only slightly outside the analytical errors for those of the whole rock ($^{206}Pb/^{204}Pb_{(t)} = 17.931$, $^{207}Pb/^{204}Pb_{(t)} = 15.569$ and $^{208}Pb/^{204}Pb_{(t)} = 37.852$) and, thus, cluster with other whole rock samples in Pb–Pb covariation diagrams (Fig. 5). Therefore, the Pb isotopic ratios of our whole rock samples appear not to have been severely affected by alteration and can be used to constrain the Pb isotopic composition of their mantle source(s).

As noted earlier, DO samples and plagioclase separate have low $\varepsilon_{Nd(t)}$ and high $^{207}Pb/^{204}Pb_{(t)}$ and $^{208}Pb/^{204}Pb_{(t)}$ for given $^{206}Pb/^{204}Pb_{(t)}$ ratios (i.e., positive Δ7/4 and Δ8/4 values), similar to those for MORB

Table 2
Pb, Nd and Sr isotope ratios and concentrations of KO and DO mafic rocks.

Karamaili mafic rocks												
Sample	KL-01	KL-03	KL-04	KL-12	KL-14	KL-15	KL-16	KL-17	KL-21	KL-24	KL-27	KL-06
Rock type	Basalt	Basalt	Basalt	Diabase	Gabbro	Gabbro	Gabbro	Gabbro	Gabbro	Basalt	Basalt	Basal andesite
Pb (ppm)	0.61	2.50	5.63	1.66	2.64	2.93	1.09	0.68	1.03	0.34	0.46	1.60
U (ppm)	0.15	0.15	0.65	0.14	0.80	2.43	0.58	0.14	0.19	0.07	0.06	1.17
Th (ppm)	0.24	0.04	1.86	0.04	0.29	0.76	0.59	0.15	0.26	0.01	0.16	3.42
$^{238}U/^{204}Pb$	15.4	3.8	7.2	5.4	19.6	54.9	34.7	13.1	11.5	12.6	6.2	48.4
$^{232}Th/^{204}Pb$	25.9	1.2	21.5	1.4	7.3	17.8	35.8	13.9	16.2	1.5	12.0	146.2
$^{206}Pb/^{204}Pb$	18.669	18.046	18.252	18.025	19.691	21.347	19.895	18.080	18.519	18.290	18.437	20.084
$^{207}Pb/^{204}Pb$	15.558	15.469	15.516	15.465	15.616	15.718	15.593	15.410	15.485	15.391	15.545	15.628
$^{208}Pb/^{204}Pb$	38.204	37.850	38.107	37.807	38.422	38.453	38.375	37.617	37.908	37.746	38.394	39.960
$^{206}Pb/^{204}Pb_{(t)}$	17.756	17.818	17.824	17.705	18.531	18.097	17.841	17.306	17.837	17.543	17.983	17.215
$^{207}Pb/^{204}Pb_{(t)}$	15.509	15.457	15.493	15.448	15.554	15.542	15.482	15.369	15.448	15.350	15.521	15.473
$^{208}Pb/^{204}Pb_{(t)}$	37.723	37.828	37.709	37.782	38.287	38.124	37.711	37.360	37.607	37.719	37.966	37.252
Δ7/4	9.4	3.5	7.1	3.8	5.5	9.1	5.8	0.3	2.5	−4.1	7.6	11.6
Δ8/4	62.9	65.9	53.3	75.0	25.6	61.8	51.4	81.0	41.5	88.2	69.5	81.2
Nd (ppm)	10.46	16.16	21.64	2.53	6.62	6.28	5.96	6.38	7.76	6.27	4.39	–
Sm (ppm)	3.36	3.49	5.54	0.99	1.73	1.68	1.73	2.13	2.13	2.18	1.50	–
$^{147}Sm/^{144}Nd$	0.1957	0.1313	0.1559	0.2377	0.1591	0.1629	0.1766	0.2031	0.1669	0.2120	0.2082	–
$^{143}Nd/^{144}Nd$	0.513132	0.513060	0.512932	0.513212	0.512922	0.512871	0.512928	0.513065	0.513023	0.513149	0.513029	–
$^{143}Nd/^{144}Nd_{(t)}$	0.512676	0.512741	0.512572	0.512658	0.512551	0.512553	0.512499	0.512475	0.512634	0.512654	0.512544	–
$\varepsilon_{Nd(t)}$	9.7	11.3	7.7	9.3	7.4	6.2	6.6	8.0	8.9	9.2	7.1	–
Sr (ppm)	615.2	349.2	349.5	224.8	291.9	543	167.1	258.6	912.8	67.39	131.2	–
Rb (ppm)	3.03	21.82	32.11	0.08	0.90	4.28	43.80	7.72	10.89	0.25	3.32	–
$^{87}Rb/^{86}Sr$	0.0143	0.1809	0.2660	0.0010	0.0089	0.0228	0.7590	0.0864	0.0345	0.0109	0.0732	–
$^{87}Sr/^{86}Sr$	0.703917	0.705040	0.705386	0.705000	0.705417	0.704809	0.707937	0.706083	0.704265	0.704356	0.705443	–
$^{87}Sr/^{86}Sr_{(t)}$	0.703844	0.704084	0.705627	0.704995	0.704862	0.703981	0.703928	0.704688	0.704088	0.704300	0.705068	–

Dalabute mafic rocks

Sample	DL-137	DL-137-pl	DL-139	DL-144	DL-145	DL-150	DL-153	DL-158	DL-159	DL-161
Rock type	Gabbro	Plagioclase	Basalt	Gabbro	Gabbro	Basalt	Basalt	Basalt	Basalt	Basalt
Pb (ppm)	2.40	4.52	2.40	0.63	0.23	0.88	0.31	0.26	0.42	0.33
U (ppm)	0.19	0.30	0.16	0.07	0.18	0.06	0.08	0.06	0.11	0.07
Th (ppm)	1.10	0.28	0.80	0.23	0.19	0.21	0.22	0.24	0.21	0.22
$^{238}U/^{204}Pb$	4.893	4.177	4.158	7.169	52.600	3.959	15.952	13.527	17.279	13.028
$^{232}Th/^{204}Pb$	29.949	4.028	21.810	23.392	56.706	15.407	47.045	60.535	32.278	42.977
$^{206}Pb/^{204}Pb$	18.221	18.194	18.184	18.383	21.078	18.122	18.514	18.387	18.449	18.750
$^{207}Pb/^{204}Pb$	15.585	15.546	15.566	15.622	15.716	15.560	15.593	15.599	15.591	15.722
$^{208}Pb/^{204}Pb$	38.407	38.069	38.314	38.477	39.013	38.258	38.559	38.837	38.538	39.154
$^{206}Pb/^{204}Pb_{(t)}$	17.932	17.946	17.938	17.958	17.962	17.888	17.569	17.585	17.425	17.978
$^{207}Pb/^{204}Pb_{(t)}$	15.569	15.533	15.553	15.599	15.548	15.547	15.542	15.555	15.536	15.680
$^{208}Pb/^{204}Pb_{(t)}$	37.852	37.995	37.910	38.044	37.962	37.972	37.687	37.716	37.940	38.358
Δ7/4	13.5	9.7	11.9	16.2	11.1	11.8	14.7	15.9	15.7	24.1
Δ8/4	54.6	67.1	59.7	70.6	61.9	71.9	82.0	82.8	124.7	99.6
Nd (ppm)	10.37		12.37	4.206	6.76	6.394	7.066	7.124	7.223	5.502
Sm (ppm)	2.777		3.665	1.587	2.48	2.143	2.305	2.362	2.365	1.789
$^{147}Sm/^{144}Nd$	0.1630		0.1803	0.2296	0.2229	0.2040	0.1985	0.2018	0.1993	0.1979
$^{143}Nd/^{144}Nd$	0.512940		0.512881	0.512904	0.513153	0.512921	0.512905	0.512883	0.512900	0.512900
$^{143}Nd/^{144}Nd_{(t)}$	0.512544		0.512443	0.512346	0.512611	0.512425	0.512422	0.512393	0.512415	0.512419
$\varepsilon_{Nd(t)}$	7.5		5.5	3.6	8.8	5.2	5.1	4.5	5.0	5.1
Sr (ppm)	448.5		550.5	569.3	172.3	84.95	488.6	263.9	109	212.5
Rb (ppm)	13.13		3.1	3.325	0.15	34.52	1.152	28.34	34.12	4.449
$^{87}Rb/^{86}Sr$	0.0848		0.0163	0.0169	0.0024	1.1767	0.0068	0.3110	0.9064	0.0606
$^{87}Sr/^{86}Sr$	0.704508		0.705503	0.705578	0.706272	0.709621	0.705953	0.707136	0.709410	0.706709
$^{87}Sr/^{86}Sr_{(t)}$	0.704060		0.705417	0.705489	0.706259	0.703406	0.705917	0.705494	0.704622	0.706389

Lead isotopic ratios were measured on a Micromass Sector 54 multicollector TIMS at the Scripps Institution of Oceanography (SIO) in a multicollector static mode using a ^{207}Pb–^{204}Pb double spike. The procedure has total blank of <100 pg Pb. The Pb isotopic compositions of each sample were adjusted to the Pb standard NBS981 values of Todt et al. (1996). The precision of Pb data is taken to be <0.03% per mass unit for $^{206}Pb/^{204}Pb$ and $^{207}Pb/^{204}Pb$ and <0.05% for $^{208}Pb/^{204}Pb$. U, Th and Pb elemental concentrations were measured on the same powder aliquots measured for Pb isotopes also do at the SIO by using a Finnigan Element 2 high-resolution inductively-coupled plasma mass spectrometer (HR-ICPMS). $^{238}U/^{204}Pb$ and $^{232}Th/^{204}Pb$ ratios are calculated from U, Th and Pb concentrations.

Strontium and Nd isotopic ratios were measured using a MC-ICPMS) at the Guangzhou Institute of Geochemistry (GIG), Chinese Academy of Sciences. Measured $^{87}Sr/^{86}Sr$ were corrected to mass fractionation using $^{86}Sr/^{88}Sr = 0.1194$. Strontium standard NBS987 was used to monitor instrumental performance and yielded an average $^{87}Sr/^{86}Sr$ ratio of 0.710242 ± 17 (2σ; n = 55). The measured $^{146}Nd/^{144}Nd$ and fractionation-corrected $^{143}Nd/^{144}Nd$ ratios of the JNdi-1 standard were 0.710288 ± 28 (2σ; n = 40) and 0.512109 ± 12 (2σ; n = 40), respectively. All measured Nd isotopic ratios were normalized to $^{146}Nd/^{144}Nd = 0.71029$. Rb, Sr, Sm and Nd were also measured at GIG. $^{147}Sm/^{144}Nd$ and $^{87}Rb/^{86}Sr$ ratios are calculated from. Rb, Sr, Sm and Nd concentrations.

Initial $^{206.\ 207.\ 208}Pb/^{204}Pb_{(t)}$, $^{143}Nd/^{144}Nd_{(t)}$ and $^{87}Sr/^{86}Sr_{(t)}$ are calculated using $^{238}U/^{204}Pb = 5$ and $^{232}Th/^{238}U = 2.3$ (White, 1993) and $^{87}Rb/^{86}Sr = 0.02$ and $^{147}Sm/^{144}Nd = 0.24$ (Mahoney et al., 1998). $\varepsilon_{Nd(t)}$ is calculated using $^{143}Nd/^{144}Nd = 0.512638$ and $^{147}Sm/^{144}Nd = 0.1967$ for present day CHUR.

Δ7/4 Pb and Δ8/4 Pb are calculated as described by Hart (1984).

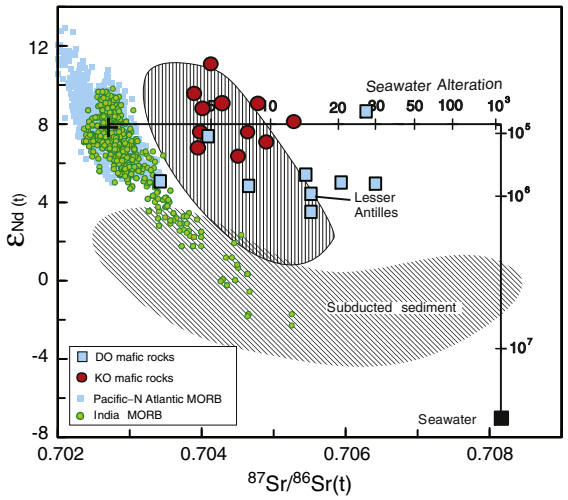

Fig. 4. Age-corrected (t = 371 Ma) $\varepsilon_{Nd(t)}$ versus $^{87}Sr/^{86}Sr_{(t)}$ ratios for KO (circles) and DO (square) mafic rocks compared to Pacific–North Atlantic and Indian MORB and convergent margin arc lavas. These are age-corrected to 371 Ma by assuming that the upper mantle MORB source has an average $^{87}Rb/^{86}Sr = 0.02$ and $^{147}Sm/^{144}Nd = 0.24$ (Mahoney et al., 1998). The solid line shows the effect of alteration on the Sr and Nd isotope composition of rocks for different water/rock ratios (crosses). Notice the shift of $^{87}Sr/^{86}Sr$ ratios towards more radiogenic values but leaving the Nd values unaffected until water/rock ratio is > 10^5. The calculation equation used is by McCulloch et al. (1981) that is modified by Faure and Mensing (2004).

$$\varepsilon_r^f = \frac{\varepsilon_r^i + \varepsilon_w^i X_W(\text{Water/Rock})}{X_r + X_w(\text{Water/Rock})}$$

The ε_r^i, ε_r^f and ε_w^i, ε_w^f are isotope ratios in the initial and final stages of rocks and water, respectively. X_r and X_w are concentrations of element X in the rocks and water. The Sr parameter used in the calculation are $\varepsilon_w^i Sr = 0.70816$ (recalculated to 371 Ma from modern seawater), $\varepsilon_w^i Sr = 0.709211$ (Veizer, 1989) and $X_w Sr = 8$ ppm; the rock value $\varepsilon_r^i Sr = 0.70270$ was recalculated to 371 Ma from the MORB value of $\varepsilon_r^i Sr = 0.70300$ (Hauff et al., 2003) and $X_r Sr = 120$ ppm. The Nd parameters used are $\varepsilon_w^i Nd = -7$ and $X_w Nd = 2.6 \times 10^{-6}$ ppm (McCulloch et al., 1981) and $\varepsilon_r^i Nd = 8$ and $X_r Nd = 10$ ppm (Hauff et al., 2003).

Data for present-day Pacific–North Atlantic and Indian MORB are from the PetDB database (http://www.petdb.org/) and the compilation of Stracke et al. (2003). Data for convergent margin arc lavas are from the GEOROC database (http://georoc.mpch-mainz.gwdg.de/georoc/).

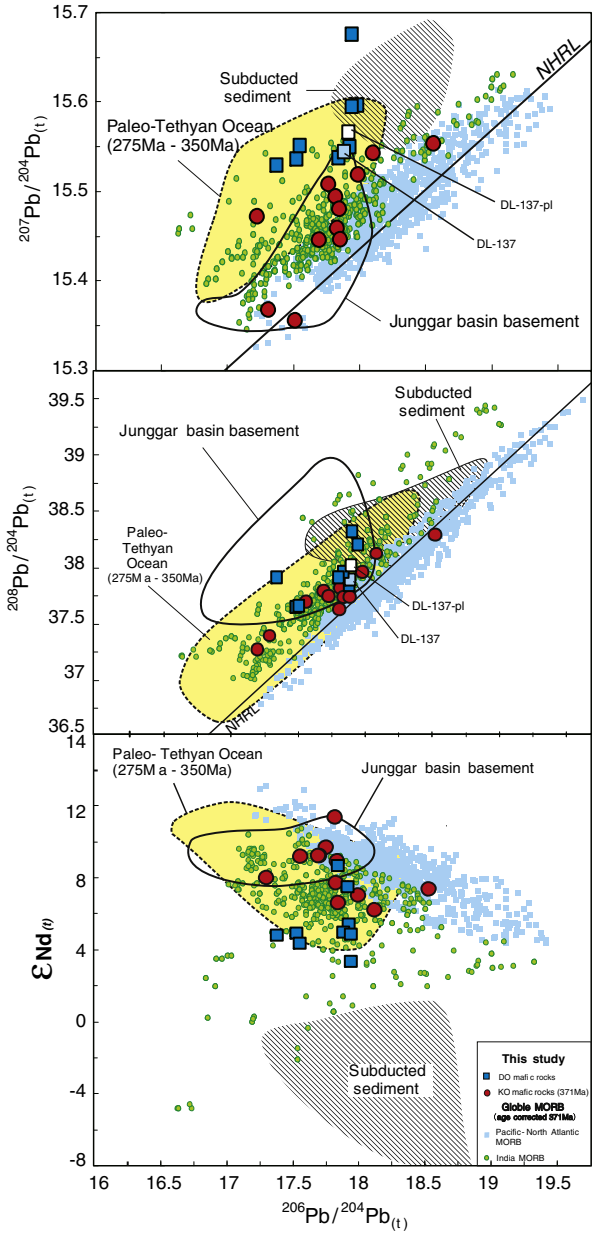

Fig. 5. Age-corrected (t = 371 Ma) $^{207}Pb/^{204}Pb_{(t)}$, $^{208}Pb/^{204}Pb_{(t)}$ and $\varepsilon_{Nd(t)}$ vs $^{206}Pb/^{204}Pb_{(t)}$ for KO and DO mafic rocks compared to age-corrected Indian and Pacific–North Atlantic MORB. Data source for MORB are the same as in Fig. 4. Age-corrected MORB field at 371 Ma was calculated by assuming $^{238}U/^{204}Pb = 5$ and $^{232}Th/^{238}U = 2.3$ in the depleted MORB source (White, 1993). Also shown are fields for Paleo-Tethyan basalts from ophiolites (Xu and Castillo, 2004; Xu et al., 2002; Zhang et al., 2005), volcanic rocks from the Junggar basin basement (Zheng et al., 2007) and subducted sediment (Plank and Langmuir, 1998). NHRL (Northern Hemisphere Reference Line) is from Hart (1984).

from the Indian Ocean. Since the trace element data indicate that DO mafic rocks came from a depleted to slightly enriched asthenospheric mantle, the combined isotopic and trace element data indicate that the DO mafic rocks most likely came from an Indian Ocean-type asthenospheric mantle with a Dupal isotopic anomaly.

The KO samples, except for sample KL-14, have a limited range of $^{206}Pb/^{204}Pb$ ratios, which additionally argues for minimal alteration effect. Sample KL-14 has a relatively high $^{206}Pb/^{204}Pb$ value most likely as a result of high degree of alteration (LOI = 10.99%). Such a high LOI value may have caused mobility of U that resulted in variation in the $^{238}U/^{204}Pb$ or μ ratio, which in turn inceases the $^{206}Pb/^{204}Pb$ ratio over time. On the other hand, although U can be mobilized, the low abundance of ^{235}U ($^{238}U/^{235}U = 137.88$) makes the $^{207}Pb/^{204}Pb$ ratio insensitive to alteration and can only be affected when substantial U is added relative to Pb (Faure and Mensing, 2004; Staudigel et al., 1996).

Similar to DO samples, KO samples have elevated $^{207}Pb/^{204}Pb$ and $^{208}Pb/^{204}Pb$ for given $^{206}Pb/^{204}Pb$ ratios, a characteristic isotopic feature of Indian MORB. The Indian MORB-type Pb isotopic signature of KO mafic rocks, however, must be treated with caution because trace element data indicate that KO mafic rocks originated from a mantle source that was contaminated by a subduction component. Interestingly, the Pb isotopic signature of Indian MORB can also be acquired from subducted, ancient marine sediments (e.g., Rehkämper and Hofmann, 1997). Addition of Pb from subducted sediment can be easily detected because of the high $^{207}Pb/^{204}Pb$ of sediment, producing a steep trend of rapidly increasing $^{207}Pb/^{204}Pb$ with increasing $^{206}Pb/^{204}Pb$ ratios. In other words, an "excess" ^{207}Pb indicates mixing of Pb between, e.g., a MORB-type, depleted mantle source and subducted sediment, which is in the form of melt and/or hydrous fluids from the subducted slab (Elliott, 2003; Elliott et al., 1997; Godard et al., 2006; Hickey-Vargas et al., 2008). Specific examples of such additions of excess ^{207}Pb are shown by magmas from the 500-Ma-old Devil River arc system in New Zealand (Münker, 2000) and for 570 Ma Agardagh Tex-Chem ophiolite in Central Asia (Pfänder et al., 2002); both examples suggest that the excess ^{207}Pb was produced by subduction of sediment derived from an Archaean source (Münker, 2000) or small amounts of old crustal material (Pfänder et al., 2002).

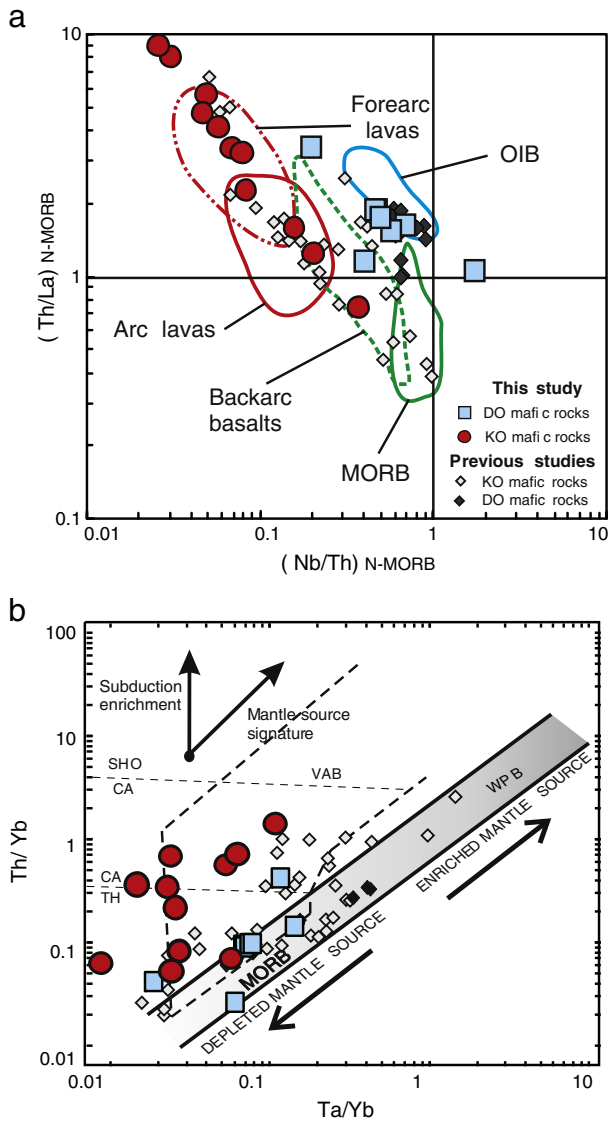

Fig. 6. Normal-MORB (Sun and McDonough, 1989) normalized (a) Th/La versus Nb/Th of KO and DO mafic rocks. The composition of bulk KO and DO mafic rocks (this and previous studies) are compared to basalts from oceanic spreading centers, seamounts, backarcs, and forearcs (MORB, OIB, backarc, arc and forearc data are from Godard et al. (2006, 2003). (b) Th/Yb versus Ta/Yb (original diagram from Pearce, 1982).
Previous data for KO and DO mafic rocks are from Lei et al. (2008), Ma (2007), Ouyang (2006), Wang et al. (2003) and Zheng et al. (2007).

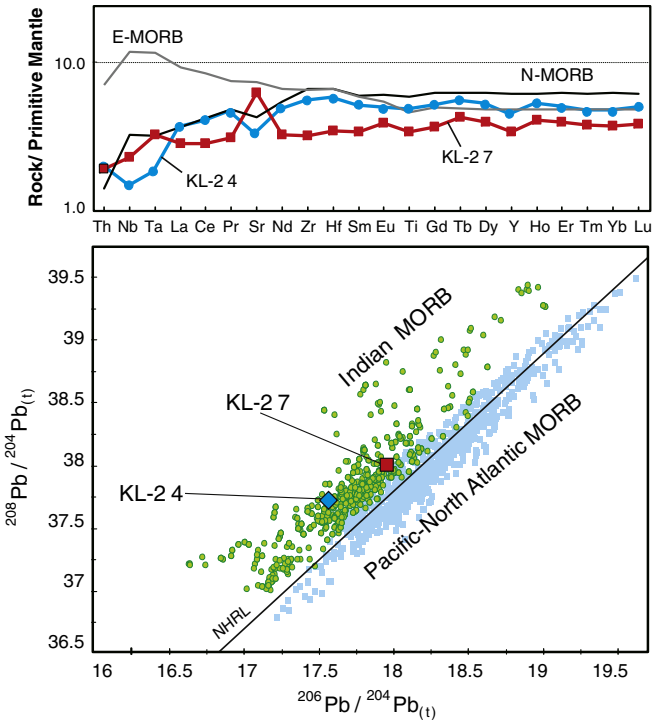

Fig. 7. Primitive mantle-normalized incompatible element concentrations and $^{208}Pb/^{204}Pb_{(t)}$ vs $^{206}Pb/^{204}Pb_{(t)}$ for KO mafic sample KL-24, 27.
Primitive mantle values are from Sun and McDonough (1989).

On the other hand, Th is immobile during alteration so that the parent/daughter (Th/Pb) ratio is generally not be affected during alteration; thus, initial $^{208}Pb/^{204}Pb$ isotope ratios of the igneous rocks should reflect those of their mantle source (Hauff et al., 2003). The well-defined correlation between $^{208}Pb/^{204}Pb$ and $^{206}Pb/^{204}Pb$ values of KO mafic rocks (Fig. 5) suggests that the KO Pb isotopic signature was most likely that of the original mantle source(s) before the subduction component addition, which is Indian MORB-like. More importantly, the Pb isotopic signature of samples KL-24 and KL-27, which have minimal influence of subduction, also indicates that the mantle source of KO mafic rocks indeed originally possessed an Indian MORB isotopic signature with a Dupal isotopic anomaly (Fig. 7), consistent with the Pb isotopic signature of DO mafic rocks. In fact, other normal-MORB-like samples from nearby PAO ophiolites also have an Indian MORB-type isotopic characteristics (Lei et al., 2008; Liu et al., 2009a, 2010). Therefore, combined with the subduction origin of the KO (e.g., Liu et al., 2007, 2009a), we propose that the KO mafic rocks were derived from an Indian MORB-type mantle that was additionally and ~recently modified by a subduction component.

To briefly summarize, our results indicate the Nd and Pb isotopic composition of PAO opholite fragments is similar to that of Indian Ocean MORB and this, in turn, suggests the existence of an Indian MORB-type mantle domain at least, beneath the southern part of the PAO since the Early Devonian. An Indian Ocean-type mantle also existed beneath the nearby Paleo-Tethyan Ocean at 275–350 Ma, and perhaps earlier (Xu and Castillo, 2004; Xu et al., 2002; Zhang et al., 2005). Thus, the Indian MORB-like characteristics of the 371 Ma KO rocks and 390 Ma DO rocks lend support to the idea that the mantle source with this isotopic signature existed prior to the opening of the present day Indian Ocean (Hickey-Vargas et al., 2008; Xu and Castillo, 2004; Xu et al., 2002; Zhang et al., 2005).

The present-day Dupal isotopic anomaly is centered in the southern hemisphere (Hart, 1984), but it also includes some parts of the Indian and Atlantic oceans in the northern hemisphere (Castillo, 1988; Regelous et al., 2009). Plate tectonic reconstruction (Scotese, 2001) showed that the Neo- and Paleo-Tethyan oceans were mainly centered in the southern hemisphere although a part of the Paleo-Tethys extended from the equator to the northern hemisphere, akin to modern Indian and Atlantic oceans. Moreover, the PAO was formed during the breakup of the Rodinia Supercontinent between 1000 and 300 Ma in the northern hemisphere (Dobretsov et al., 1995, 2003). In particular, the Junggar Ocean, which represents the southern branch of PAO, was located from 0° N to 40° N (Klootwijk, 2013; Windley et al., 2007; Xiao et al., 2010). If these are all true, then our isotopic data combined with previous results (e.g., Xu and Castillo, 2004; Xu et al., 2002) indicate that the Dupal isotopic anomaly was present in the sub-oceanic mantle beneath the Neo- and Paleo-Tethys in the southern hemisphere and in the Junggar Ocean in the northern hemisphere.

Goldstein et al. (2008) summarized all possible origins of the Dupal anomaly, including upwelling of the lower mantle through plumes (Castillo, 1988) followed by contamination of the asthenosphere by such mantle plumes (e.g., Class and le Roex, 2011; Weis and Frey,

Table 3
Model parameter used for mixing model calculation.

	Partition coefficients		
	D_{Th}	D_{Nd}	D_{Pb}
Sediment/melt[a]	0.89	1.53	1.29
Sediment/fluid[a]	–	3.26	0.64
AOC/fluid[b]	–	51	0.1
	Trace elements (ppm)		
	Th	Nd	Pb
DIMM[c]	0.004	0.483	0.014
Sediment[d]	6.91	27	19.9
Sediment melt[e]	7.72	17.96	15.6
LAOC (KL-14)[f]	–	6.62	2.64
Sediment fluid[g]	–	8.24	30.92
LAOC fluid[h]	–	0.13	24.22
Slab fluid[i]	–	1.75	25.56

	Isotopic compositions			
0 Ma	$^{143}Nd/^{144}Nd_{(0)}$	$^{206}Pb/^{204}Pb_{(0)}$	$^{207}Pb/^{204}Pb_{(0)}$	$^{208}Pb/^{204}Pb_{(0)}$
DIMM[j]	0.51326	17.90	15.46	37.77
Sediment (GLOSS)[k]	0.51218	–	–	–
Sediment melt (GLOSS)[k]	0.51218	–	–	–
Sediment (unradiogenic Pb)[l]	0.51231	18.82	15.65	38.92
Sediment melt (unradiogenic Pb)[l]	0.51231	18.82	15.65	38.92

Age-corrected to 371 Ma	$^{143}Nd/^{144}Nd_{(t)}$	$^{206}Pb/^{204}Pb_{(t)}$	$^{207}Pb/^{204}Pb_{(t)}$	$^{208}Pb/^{204}Pb_{(t)}$	$\varepsilon_{Nd(t)}$
DIMM[j]	0.51267	17.18	15.35	37.22	10.0
Sediment (GLOSS)[k]	0.51186	–	–	–	–
Sediment melt (GLOSS)[k]	0.51186	–	–	–	–
Sediment (unradiogenic Pb)[l]	0.51196	18.15	15.61	38.48	−3.9
Sediment melt (unradiogenic Pb)[l]	0.51196	18.15	15.61	38.48	−3.9
Slab fluid[m]	0.51255	18.53	15.55	38.29	7.3

[a] Sediment/melt and sediment/fluid partition coefficients from Johnson and Plank (1999).
[b] AOC/fluid partition coefficients calculated from Brenan et al. (1995a, 1995b) by assuming subducted oceanic crust has garnet:cpx = 60:40.
[c] DIMM trace element concentration values are from Workman and Hart (2005).
[d] Sediment trace element concentration values are from GLOSS (Plank and Langmuir, 1998).
[e] Calculated sediment melt trace element composition assuming 5% of melting of GLOSS (Plank and Langmuir, 1998) and partition coefficient in note a.
[f] LAOC trace element values are represented by highly altered sample KL-14 (LOI = 10.99%) from Liu et al. (2007).
[g] Calculated trace element composition of fluid released during dehydration of subducted sediment (GLOSS) (Plank and Langmuir, 1998). This assumes 1% of fluid in equilibrium with sediment and partition coefficient in note a.
[h] Calculated trace element composition of fluid released from LAOC as noted f. This assumes 1% of fluid in equilibrium with LAOC and partition coefficient in note b.
[i] Calculated trace element composition of slab fluid assumes a 80:20 mixture of LAOC:sediment-derived fluids.
[j] Neodymium isotopic values of DIMM are from Workman and Hart (2005). Pb isotopic values are from Indian MORB compiled from Stracke et al. (2003) and PetDB database (website: http://www.petdb.org/). DIMM age-corrected Isotope values are calculated by assuming $^{87}Rb/^{86}Sr = 0.02$ and $^{147}Sm/^{144}Nd = 0.24$ (Mahoney et al., 1998), and $^{238}U/^{204}Pb = 5$ and $^{232}Th/^{238}U = 2.3$ in the depleted MORB source (White, 1993). $\varepsilon_{Nd(t)}$ is calculated using $^{143}Nd/^{144}Nd = 0.512638$ and $^{147}Sm/^{144}Nd = 0.1967$ for present day CHUR.
[k] Sediment (GLOSS) Nd isotopic values are from Plank and Langmuir (1998), age-corrected to 371 Ma are calculate by using trace element concentration of GLOSS: Sm = 5.78 ppm and Nd = 27 ppm.
[l] Sediment (unradiogenic Pb) Nd and Pb isotopic values are from Izu–Bonin sediment (Plank and Langmuir, 1998; Plank et al., 2007). Age-corrected to 371 Ma are calculate by using trace element concentration of average Izu–Bonin sediment: Sm = 6.35 ppm, Nd = 28.7 ppm, Pb = 6.82 ppm, U = 1.19 ppm and Th = 2.43 ppm (Plank and Langmuir, 1998). $\varepsilon_{Nd(t)}$ calculated as note j.
[m] Slab fluid Nd and Pb isotopic values are represented by highly altered sample KL-14 (LOI = 10.99%) from Liu et al. (2007).

1996) and mantle modification either through focused subduction (Staudigel et al., 1996) of altered oceanic crust and sediment (Rehkämper and Hofmann, 1997) or through recycling of arc crust (Kempton et al., 2002) or detached sub-continental lithospheric mantle (SCLM) during continental break-up (Chung et al., 2001; Hanan et al., 2004; Mahoney et al., 1998). Therefore, the exact origin of the anomaly is still a contentious issue. Our new results cannot exclude any of the competing models for the exact origin of the isotopically anomalous regions in the lower mantle. However, our results reinforce the idea that the distinct Indian MORB-type (i.e., Dupal) isotopic signature is an asthenospheric feature and it is produced through contamination by upwelling plumes carrying materials from the deep mantle (e.g., Weis and Frey, 1996).

In summary, we propose that the long-lived Dupal isotopic anomaly of the Indian Ocean-type mantle domain was ultimately derived from the lower mantle although some of its geochemical features may have been modified by relatively more recent, shallow mantle geological processes such as lithospheric delamination or subduction. Our data, however, cannot constrain the exact origin of the isotopically anomalous lower mantle. More investigations, particularly of ancient (>390 Ma) ophiolites, are needed in order to resolve this important problem.

6.2. The subduction component

6.2.1. Subducted sediment

As discussed above, trace element and isotopic data indicate that the DO mafic rocks most likely came from an Indian MORB-type asthenospheric mantle whereas the KO mafic rocks came from a similar source that had been additionally contaminated during a relatively ~recent subduction event (e.g., Liu et al., 2007, 2009a). Here we further discuss the nature of the subduction component and quantify its influence on the Indian MORB-type mantle source of the KO mafic samples. To constrain its nature, we first investigate the behavior of Th/Nd ratios against $^{143}Nd/^{144}Nd$ ratio of KO mafic samples to evaluate sediment melt

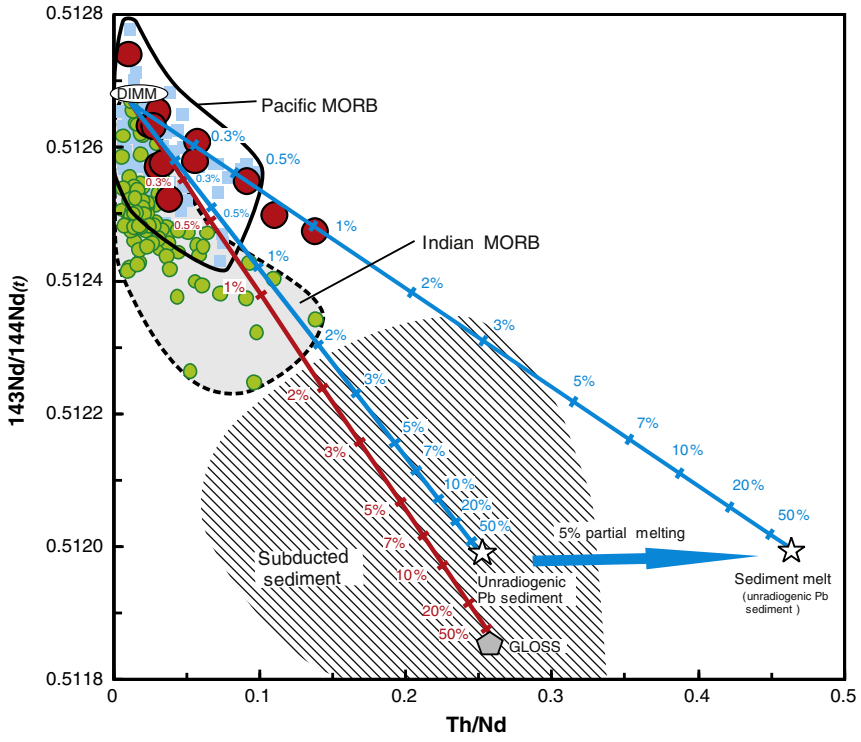

Fig. 8. Plot of Th/Nd versus $^{143}Nd/^{144}Nd_{(t)}$ for KO mafic rocks. KO mafic rocks form a binary linear array between mantle wedge and sediment components. The mantle wedge end-member was assumed to be a very depleted-Indian MORB mantle (DIMM; Stracke et al., 2003) with high $^{143}Nd/^{144}Nd_{(t)}$ but low Th/Nd ratios. The low $^{143}Nd/^{144}Nd_{(t)}$ and high Th/Nd ratio end-member is interpreted to be bulk sediment or sediment melt calculated in Table 3. Note that the global subducted sediment (GLOSS; Plank and Langmuir, 1998) and its melts were not appropriate for explaining the entire compositional spectrum of KO mafic rocks. Thus, we assumed that the PAO sediment would have unradiogenic Pb isotopes, similar to present day sediment in the Izu–Bonin trench (Plank and Langmuir, 1998; Plank et al., 2007). Results of calculation indicate that addition of ≤1% of this sediment partial melt to DIMM can account for the subduction component signature of KO mafic rocks. Tick marks on the calculated DIMM-sediment (melt) mixing lines are labeled with wt.% of sediment (melt). Data source are same the same as in Fig. 4. Partition coefficients of the sediment melt are in Table 3 and explained in the text.

contribution to a depleted mantle source. We use Th and Nd because these are immobile in fluid dehydrated from subducted oceanic crust and sediment, but are relatively mobile in sediment melt (Class et al., 2000; Elliott et al., 1997; Johnson and Plank, 1999). Moreover, Th is more incompatible ($D^{Th}_{sediment/melt} = 0.89$) than Nd ($D^{Nd}_{sediment/melt} = 1.53$) during melting (Johnson and Plank, 1999) and, thus, a sediment partial melt could fractionate the Th/Nd ratio from the bulk sediment. We assume a depleted-Indian MORB mantle (DIMM; compiled from Stracke et al., 2003) as the mantle end-member. For the sediment end-member, we first use the global subducted sediment (GLOSS; Plank and Langmuir, 1998), and results of all our calculations, presented below, show that GLOSS does constitute an appropriate sediment end-member. Previous studies have suggested that the PAO was surrounded by active margins and many pieces of PAO crust similar to KO were most probably exposed along these margins (Dobretsov et al., 1995; Jahn, 2004; Sengör et al., 1993; W.J. Xiao et al., 2009). This is especially evident in the southern CAOB as it is mainly comprised of juvenile mantle-derived materials (Jahn, 2004; Sun et al., 2008). Consequently, sediments derived from these margins would have unradiogenic Pb but radiogenic Nd isotopes. Among present-day subducted sediments (Plank and Langmuir, 1998; Plank et al., 2007), sediment from the Izu–Bonin trench has the least radiogenic Pb and radiogenic Nd isotopes, and incidentally its provenance is connected to an Indian MORB type mantle (Tollstrup et al., 2010). Thus, the Izu–Bonin sediment represents a realistic sediment end-member.

We use a simple two-component mixing model and the parameters in Table 3 to calculate the relative proportions of the depleted mantle and bulk sediment end-members in the source of KO mafic samples. Results of our calculations (Fig. 8) show that, except for one sample, mixing of bulk Izu–Bonin sediment and DIMM simply cannot produce the high Th/Nd for given $^{143}Nd/^{144}Nd$ of the bulk of the mafic samples. In order to explain the spectrum of Th/Nd for given $^{143}Nd/^{144}Nd$ values of the bulk of the samples, we have to elevate the Th/Nd ratio of the bulk sediment first by partial melting (see also, Class et al., 2000; Singer et al., 2007). By iteration, we found that the sediment needs to be partially melted by ~5 wt.% in order to cover the range of Th/Nd and $^{143}Nd/^{144}Nd$ ratios of the bulk of KO mafic rocks. Addition of ≤1% of this sediment partial melt to a highly depleted mantle source can account for the subduction component signature of KO mafic rocks.

6.2.2. Dehydration fluid

Many investigators believe that the subduction component consists primarily of hydrous fluid dehydrated from subducted altered oceanic crust and only a lesser amount of melt from subducted sediment (e.g., Plank and Langmuir, 1998; Turner and Hawkesworth, 1997). Thus, it is reasonable to assume that dehydration fluid, in addition to sediment melt discussed above, was also a part of the subduction component that influenced the source of KO mafic rocks. Thus, to further constrain the nature of subduction component in the mantle source of KO mafic rocks, we use both Nd and Pb isotopes to evaluate the importance of the dehydrated fluid in the slab component. Neodymium and Pb isotopes provide powerful constraints because they combine the relatively hydrous fluid-immobile character of Nd with hydrous fluid mobile character of Pb. For the model calculations, we use the same depleted mantle and sediment melt end-members as in the previous sediment melt model (Table 3). For the fluid end-member, we use the isotopic composition of the highly altered basalt sample KL-14 (LOI = 10.99%) of local altered oceanic crust (LAOC); for trace element composition, we mix 80% of fluid released from LAOC sample KL-14 with 20% fluid released from sediment (see Table 3).

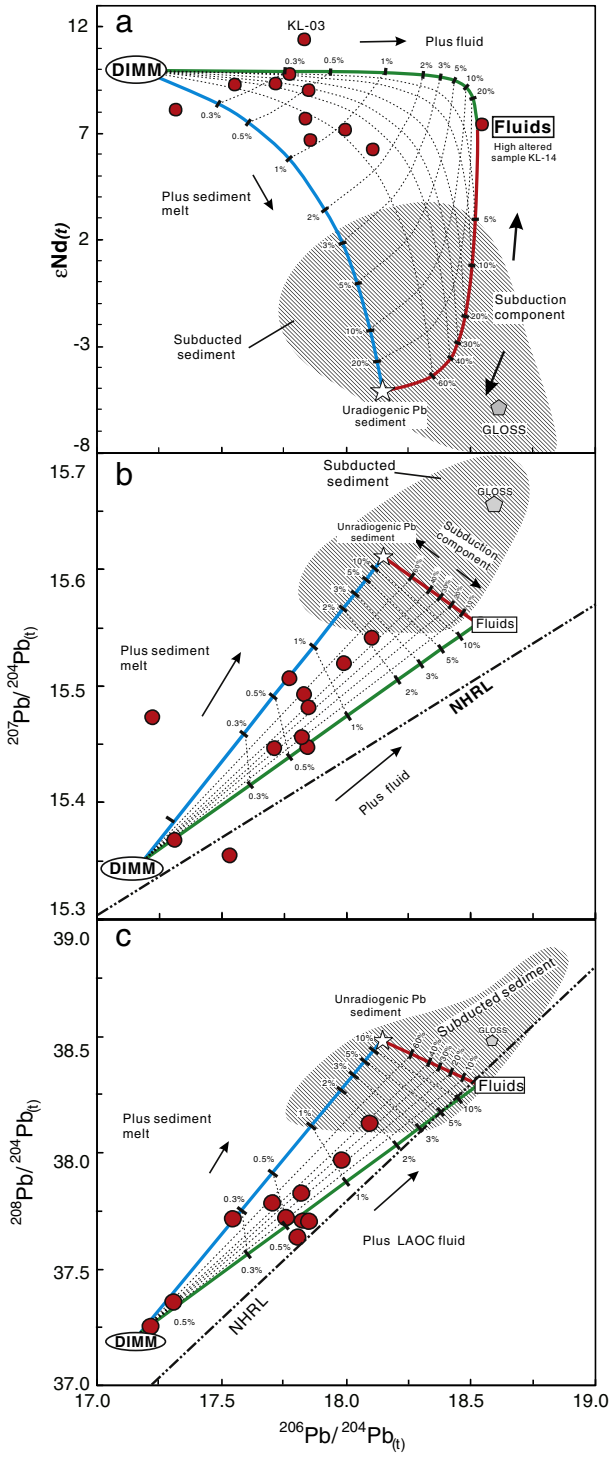

Fig. 9. Diagrams of $\varepsilon_{Nd(t)}$, $^{207}Pb/^{204}Pb_{(t)}$ and $^{208}Pb/^{204}Pb_{(t)}$ versus $^{206}Pb/^{204}Pb_{(t)}$ showing the amounts of Nd and Pb in the subduction component that affected the KO sub-mantle. Partition coefficients and compositions of fluid from local altered oceanic crust (LAOC), sediment, and sediment melt are listed in Table 3 and explained in the text. Values for the subducted sediment and DIMM are the same as Fig. 8. Mixing lines between DIMM and fluid from LAOC and subducted sediment, DIMM and sediment melt, and especially between fluids and sediment melt indicate the isotopic composition of the subduction component (SC). Mixing calculation results suggest that the compositional array of the sub-KO mantle cannot be explained by mixing a SC that is either purely sediment or purely fluid; instead, the SC is a variable mixture of sediment and fluid; addition ≤2% of such a SC is consistent with the data. Symbols as in Fig. 8. Tick marks on the calculated mixing lines are labeled in wt.% of individual end-members.

Our model calculation results show that the bulk of KO mafic rocks are inside the area defined by the depleted mantle, sediments melt and fluid (Fig. 9). None of the samples has a subduction component that is either purely sediment or purely fluid; instead, the subduction component is a variable mixture of the two. Moreover, the subduction component flux to the depleted mantle wedge is variable because the amount of sediment subducted, the extent of partial melting of such sediment, amount of slab dehydration, and other factors such as temperature, pressure, water content, and oxidation state in the subduction zone (Kelley and Cottrell, 2009; Kelley et al., 2006) are also variable. In any case, the total amount of subduction component that mixed with the depleted mantle to generate the range of mantle sources of the parental melts of KO mafic samples in all model calculations is consistently ≤2%. Note that this combined fluid and sediment contribution to the subduction component is higher than sediment melt contribution alone (Fig. 8). Moreover, this is an upper limit of subduction component contribution as some of the KO mafic rocks (i.e., group 2 samples) may have been derived from a slightly enriched mantle source to begin with. The main point of these simple exercises using refractory elements and Nd and Pb isotopes is simply to show that subducted sediment and fluid dehydrated from altered oceanic crust are needed to produce the subduction component that influenced the mantle source of KO parental magmas.

7. Conclusions

Results of our combined major-trace element and Nd and Pb isotopic investigation suggest a common, Indian MORB-type mantle source for DO and KO mafic rocks. Thus, the isotopically Indian MORB-type upper mantle with a Dupal isotopic anomaly had been in existence since at least ~390 Ma ago beneath the PAO. This lends support to the idea that the Dupal isotopic anomaly existed prior to the opening of the Indian Ocean. However, the composition of portions of the KO mantle was additionaly influenced by a relatively ~recent subduction process, which, importantly, can also produce a Dupal-like isotopic signature. Thus, caution must be taken when interpreting Dupal isotopic signals coming from ancient ophiolities. Model calculations for KO mafic rocks indicate that ≤2% of subduction component consisting of a variable mixture of ~5% partial melt of sediment with unradiogenic Pb sediment and fluid dehydrated from altered oceanic crust was added to the depleted Indian mantle to produce KO parental magmas.

We conclude that the Dupal isotopic signature is a long-lived asthenospheric feature that existed beneath the Neo- and Paleo-Tethyan Ocean (275–350 Ma) in the southern hemisphere and in the southern section of PAO (371–390 Ma) in the northern hemisphere. The Dupal isotopic signature of the asthenosphere was most likely produced through contamination by upwelling plumes of an isotopically unusual deep mantle component generated through ancient subduction or delamination of lithospheric materials.

Acknowledgments

We are grateful for constructive reviews by M. Sun, another one anonymous referee and editors that led to clarification and improvement of the manuscript. We also thank Liyan Tian and Chris MacIsaac for their help in the isotopic analysis. This study was jointly supported by NSFC funds (No. 41302041; 40930316; 41230207; 40425003), Guangxi National Natural Science Foundation of China (No. 2012GXNSFCA053007), China Postdoctoral Science Foundation Grant (2013M530440), open research grants of Guangxi Key Laboratory of Hidden Metallic Ore Deposits Exploration (No. 13-A-01-01) and the State Key Laboratory for Mineral Deposits Research (Nanjing University) (18-13-6), Bagui Scholar Innovation Project of Guangxi Province (to Xu Jifeng), research grants of GUT and China Scholarship Council Fund Ph.D. Study Abroad Program (2008). Part of this study was done by X. L. as a

visiting graduate student at the Scripps Institution of Oceanography, University of California, San Diego. This is a contribution to IGCP 592.

References

Brenan, J.M., Shaw, H.F., Ryerson, F.J., Phinney, D.L., 1995a. Experimental determination of trace-element partitioning between pargasite and a synthetic hydrous andesitic melt. Earth and Planetary Science Letters 135, 1–11.

Brenan, J.M., Shaw, H.F., Ryerson, F.J., Phinney, D.L., 1995b. Mineral–aqueous fluid partitioning of trace elements at 900 °C and 2.0 GPa: constraints on the trace element chemistry of mantle and deep crustal fluids. Geochimica et Cosmochimica Acta 59, 3331–3350.

Bu, G.M., Liu, H.Q., Li, W.Q., Yu, H.X., Jin, H., 2005. Geochemical characteristics and tectonic setting for basalts in Takezhale ophiolite in East Junggar, Xingjiang. Geotectonica et Metallogenia 29, 252–261.

Cai, W., 1986. Preliminary study of plate tectonics of northern east Junggar in Xinjiang Uygur Autonomous Region. Contributions of the Project of Plate Tectonics in Northern China, No.1. Geological Publishing House, Beijing 1–23.

Castillo, P., 1988. The Dupal anomaly as a trace of the upwelling lower mantle. Nature 336, 667–670.

Chen, J.-L., Zhao, W.-X., Xu, J.-F., Wang, B.-D., Kang, Z.-Q., 2012. Geochemistry of Miocene trachytes in Bugasi, Lhasa block, Tibetan Plateau: mixing products between mantle- and crust-derived melts? Gondwana Research 21, 112–122.

Chung, S., Sun, S., Crawford, A., 2001. Indian Ocean type convecting mantle underlies East Asia: a consequence of Gondwana breakup and reassembly? Western Pacific Earth Sciences 1, 1–18.

Class, C., le Roex, A., 2011. South Atlantic DUPAL anomaly — dynamic and compositional evidence against a recent shallow origin. Earth and Planetary Science Letters 305, 92–102.

Class, C., Miller, D.M., Goldstein, S.L., Langmuir, C.H., 2000. Distinguishing melt and fluid subduction components in Umnak Volcanics, Aleutian Arc. Geochemistry, Geophysics, Geosystems 1.

Coleman, R.G., 1989. Continental growth of northwest China. Tectonics. AGU, pp. 621–635.

Condie, K.C., 2003. Incompatible element ratios in oceanic basalts and komatiites: tracking deep mantle sources and continental growth rates with time. Geochemistry, Geophysics, Geosystems 4.

Dilek, Y., 2003. Ophiolite concept and its evolution. In: Dilek, Y., Newcomb, S. (Eds.), Geological Society of America Special Paper 373: Ophiolite Concept and the Evolution of Geological Thought, pp. 1–16.

Dobretsov, N.L., Berzin, N.A., Buslov, M.M., 1995. Opening and tectonic evolution of the Paleo-Asian ocean. International Geology Review 37, 335–360.

Dobretsov, N.L., Buslov, M.M., Vernikovsky, V.A., 2003. Neoproterozoic to Early Ordovician evolution of the Paleo-Asian Ocean: implications to the break-up of Rodinia. Gondwana Research 6, 143–159.

Dupre, B., Allegre, C.J., 1983. Pb–Sr isotope variation in Indian Ocean basalts and mixing phenomena. Nature 303, 142–146.

Elliott, T., 2003. Tracers of the Slab, Inside the Subduction Factory.AGU, Washington, DC 23–45.

Elliott, T., Plank, T., Zindler, A., White, W., Bourdon, B., 1997. Element transport from slab to volcanic front at the Mariana arc. Journal of Geophysical Research 102, 14991–15019.

Faure, G., Mensing, T., 2004. Isotopes: Principles and Applications.John Wiley & Sons Inc.

Godard, M., Dautria, J.-M., Perrin, M., 2003. Geochemical variability of the Oman ophiolite lavas: relationship with spatial distribution and paleomagnetic directions. Geochemistry, Geophysics, Geosystems 4.

Godard, M., Bosch, D., Einaudi, F., 2006. A MORB source for low-Ti magmatism in the Semail ophiolite. Chemical Geology 234, 58–78.

Goldstein, S.L., Soffer, G., Langmuir, C.H., Lehnert, K.A., Graham, D.W., Michael, P.J., 2008. Origin of a 'Southern Hemisphere' geochemical signature in the Arctic upper mantle. Nature 453, 89–93.

Gu, P., Li, Y., Zhang, B., Tong, L., Wang, J., 2009. LA-ICP-MS zircon U–Pb dating of gabbro in the Darbut ophiolite, West Junggar, China. Acta Petrologica Sinica 25, 1364–1372.

Hamelin, B., Allegre, C.J., 1985. Large-scale regional units in the depleted upper mantle revealed by an isotope study of the South-West Indian Ridge. Nature 315, 196–199.

Hanan, B.B., Blichert-Toft, J., Pyle, D.G., Christie, D.M., 2004. Contrasting origins of the upper mantle revealed by hafnium and lead isotopes from the Southeast Indian Ridge. Nature 432, 91–94.

Hart, S.R., 1984. A large-scale isotope anomaly in the Southern Hemisphere mantle. Nature 309, 753–757.

Hauff, F., Hoernle, K., Schmidt, A., 2003. Sr–Nd–Pb composition of Mesozoic Pacific oceanic crust (Site 1149 and 801, ODP Leg 185): implications for alteration of ocean crust and the input into the Izu–Bonin–Mariana subduction system. Geochemistry, Geophysics, Geosystems 4.

Hawkins, J.W., 2003. Geology of supra-subduction zones—implications for the origin of ophiolites. In: Dilek, Y., Newcomb, S. (Eds.), Geological Society of America Special Paper 373: Ophiolite Concept and the Evolution of Geological Thought, pp. 227–268.

He, G., Li, M., Jia, J., Zhou, H., 2000. A discussion on age and tectonic significance of ophiolite in eastern Junggar, Xinjiang. Acta Scientiarum Naturalium Universitatis Pekinensis 37, 852–858.

Helo, C., Hegner, E., Kroner, A., Badarch, G., Tomurtogoo, O., Windley, B.F., Dulski, P., 2006. Geochemical signature of Paleozoic accretionary complexes of the Central Asian Orogenic Belt in South Mongolia: constraints on arc environments and crustal growth. Chemical Geology 227, 236–257.

Hickey-Vargas, R., Bizimis, M., Deschamps, A., 2008. Onset of the Indian Ocean isotopic signature in the Philippine Sea Plate: Hf and Pb isotope evidence from Early Cretaceous terranes. Earth and Planetary Science Letters 268, 255–267.

Jahn, B.-M., 2004. The Central Asian Orogenic Belt and growth of the continental crust in the Phanerozoic. Geological Society, London, Special Publications 226, 73–100.

Jian, P., Liu, D., Yuruo, S., Fuqin, Z., 2005. SHRIMP dating of SSZ ophiolites from northern Xinjiang Province, China — implications for generation of oceanic crust in the Central Asian Orogenic Belt. In: Sklyarov, E.V. (Ed.), Structural and Tectonic Correlation Across the Central Asia Orogenic Collage: North-Eastern Segment, Guidebook and Abstract Volume of the Siberian Workshop ICCP-480. ICE SBRAS, Irkutsk, p. 246.

Johnson, M.C., Plank, T., 1999. Dehydration and melting experiments constrain the fate of subducted sediments. Geochemistry, Geophysics, Geosystems 1.

Kawahata, H., Nohara, M., Ishizuka, H., Hasebe, S., Chiba, H., 2001. Sr isotope geochemistry and hydrothermal alteration of the Oman ophiolite. Journal of Geophysical Research 106.

Kelley, K.A., Cottrell, E., 2009. Water and the oxidation state of subduction zone magmas. Science 325, 605–607.

Kelley, K.A., Plank, T., Grove, T.L., Stolper, E.M., Newman, S., Hauri, E., 2006. Mantle melting as a function of water content beneath back-arc basins. Journal of Geophysical Research 111, B09208.

Kempton, P.D., Pearce, J.A., Barry, T.L., Fitton, J.G., Langmuir, C., Christie, D.M., 2002. Sr–Nd–Pb–Hf isotope results from ODP Leg 187: evidence for mantle dynamics of the Australian–Antarctic discordance and origin of the Indian MORB source. Geochemistry, Geophysics, Geosystems 3.

Klootwijk, C., 2013. Middle–Late Paleozoic Australia–Asia convergence and tectonic extrusion of Australia. Gondwana Research 24, 5–54.

Le Bas, M., Maitre, R., Streckeisen, A., Zanettin, B., 1986. A chemical classification of volcanic rocks based on the total alkali–silica diagram. Journal of Petrology 27, 745–750.

Lei, M., Zhao, Z.D., Hou, Q.Y., Zhang, H.F., Xu, J.F., Chen, Y.L., Zhang, B.R., Liu, X.J., 2008. Geochemical and Sr–Nd–Pb isotopic characteristics of the Dalabute ophiolite, Xinjiang: comparison between the Paleo-Asian ocean and the Tethyan mantle domains. Acta Petrologica Sinica 24, 661–672.

Li, J., 1995. Main characteristics and emplacement processes of the east Junggar ophiolites, Xinjiang, China. Acta Petrologica Sinica 11, 73–84 (Suppl.).

Li, X.H., 1997. Geochemistry of the Longsheng ophiolite from the southern margin of Yangtze craton, SE China. Geochemical Journal 31, 323–337.

Li, J., Xiao, W., Wang, K., Sun, G., Gao, L., 2003. Neoproterozoic–Paleozoic tectonostratigraphy, magmatic activities and tectonic evolution of eastern Xinjiang, NW China. In: Mao, J.W., Goldfarb, R.J., Seltmann, R., Wang, D.H., Xiao, W.J., Hart, C. (Eds.), Tectonic Evolution and Metallogeny of the Chinese Altay and Tianshan, London, IAGOD Guidebook Series, pp. 31–74.

Liang, X.R., Wei, G.J., Li, X.H., Liu, Y., 2003. Precise determination of $^{143}Nd/^{144}Nd$ and Sm/Nd ratios using multiple-collector inductively coupled plasma mass spectrometer (MC-ICPMS). Geochimica 32, 91–96.

Liu, X.J., Liao, S., 2012. High precision Pb isotope determination by using ^{207}Pb–^{204}Pb double spike revisited. Advanced Materials Research 518, 1669–1676.

Liu, X.J., Xu, J.F., Hou, Q.Y., Bai, Z.H., Lei, M., 2007. Geochemical characteristics of Karamaili ophiolite in east Junggar, Xingjiang: products of ridge subduction. Acta Petrologica Sinica 23, 1591–1602.

Liu, X.J., Castillo, P.R., Xu, J.F., Hou, Q.Y., 2009a. The Dupal isotope anomaly in the Paleo-Asian sub-oceanic mantle: Nd–Sr–Pb isotope evidence from ophiolites in Northern China. American Geophysical Union, Fall Meeting AGU, San Fransisco (pp. abstract #V33C-2048).

Liu, X.J., Castillo, P.R., Xu, J.F., Hou, Q.Y., 2009b. Geochemistry and rock association in the Karamaili Paleo-Asian ophiolite in east Junggar, NW China suggest ridge–trench interaction. Geochimica et Cosmochimica Acta 73, A782.

Liu, X.J., Xu, J.F., Wang, S.Q., Hou, Q.Y., Bai, Z.H., Lei, M., 2009c. Geochemistry and dating of E-MORB type mafic rocks from Dalabute ophiolite in West Junggar, Xinjiang and geological implications. Acta Petrologica Sinica 25, 1373–1389.

Liu, X.J., Castillo, P.R., Xu, J.F., Hou, Q.Y., 2010. The Dupal isotope anomaly in the Paleo-Asian sub-oceanic mantle: Nd–Sr–Pb isotope evidence from ophiolites in Northern China. Geochimica et Cosmochimica Acta 74, A622.

Liu, X.J., Wang, G.Q., Castillo, P.R., Xu, J.F., Huang, F., Yu, H.X., Chen, L., 2013. Highly precise Pb isotope analysis by ^{207}Pb–^{204}Pb double spike method using TIMS. Geochimica 42, 103–115.

Ma, Z.P., 2007. Research of Ophiolite from Tienshan and Adjacent Areas and Evolutionary Processes of Paleozoic Oceans, Northwest Xinjiang. (Ph.D. thesis) Northwest University, Xi'an 126.

Mahoney, J., le Roex, A.P., Peng, Z., Fisher, R.L., Natland, J.H., 1992. Southwestern limits of Indian Ocean Ridge Mantle and the origin of low $^{206}Pb/^{204}Pb$ mid-ocean ridge basalt: isotope systematics of the central Southwest Indian Ridge (17°–50°E). Journal of Geophysical Research 97, 19771–19790.

Mahoney, J.J., Frei, R., Tejada, M.L.G., Mo, X.X., Leat, P.T., NäGler, T.F., 1998. Tracing the Indian Ocean mantle domain through time: isotopic results from old west Indian, east Tethyan, and South Pacific seafloor. Journal of Petrology 39, 1285–1306.

Mahoney, J.J., Graham, D.W., Christie, D.M., Johnson, K.T.M., Hall, L.S., Vonderhaar, D.L., 2002. Between a hotspot and a cold spot: isotopic variation in the Southeast Indian Ridge asthenosphere, 86°E–118°E. Journal of Petrology 43, 1155–1176.

McCulloch, M.T., Gregory, R.T., Wasserburg, G.J., Taylor Jr., H.P., 1981. Sm–Nd, Rb–Sr, and $^{18}O/^{16}O$ isotopic systematics in an oceanic crustal section: evidence from the Samail ophiolite. Journal of Geophysical Research 86, 2721–2735.

Miyashiro, A., 1974. Volcanic rock series in island arcs and active continental margins. American Journal of Science 274, 321–355.

Moores, E.M., Jackson, E.D., 1974. Ophiolites and oceanic crust. Nature 250, 136–139.

Münker, C., 2000. The isotope and trace element budget of the Cambrian Devil River Arc System, New Zealand: identification of four source components. Journal of Petrology 41, 759–788.
Ouyang, Z.J., 2006. Research of Paleozoic Tectonic Process in Northeast Xinjiang. (Ph.D. thesis) Department of Geology, Northwest University, Xi'an, China 144.
Pearce, J., 1982. Trace Element Characteristics of Lavas from Destructive Plate Margins. Andesites: Orogenic Andesites and Related Rocks.Wiley, New York 525–548.
Pearce, J.A., Peate, D.W., 1995. Tectonic implications of the composition of volcanic ARC magmas. Annual Review of Earth and Planetary Sciences 23, 251–285.
Pearce, J.A., Lippard, S.J., Roberts, S., 1984. Characteristics and tectonic significance of supra-subduction zone ophiolites. Geological Society, London, Special Publications 16, 77–94.
Peate, D.W., Pearce, J.A., 1998. Causes of spatial compositional variations in Mariana arc lavas: trace element evidence. The Island Arc 7, 479–495.
Pfänder, J., Jochum, K., Kozakov, I., Kröner, A., Todt, W., 2002. Coupled evolution of back-arc and island arc-like mafic crust in the late-Neoproterozoic Agardagh Tes-Chem ophiolite, Central Asia: evidence from trace element and Sr–Nd–Pb isotope data. Contributions to Mineralogy and Petrology 143, 154–174.
Plank, T., Langmuir, C.H., 1998. The chemical composition of subducting sediment and its consequences for the crust and mantle. Chemical Geology 145, 325–394.
Plank, T., Kelley, K.A., Murray, R.W., Stern, L.Q., 2007. Chemical composition of sediments subducting at the Izu–Bonin trench. Geochemistry, Geophysics, Geosystems 8, Q04I16.
Presnall, D., Hoover, J., 1987. High pressure phase equilibrium constraints on the origin of mid-ocean ridge basalts. In: Mysen, B.O. (Ed.), Magmatic Processes: Physicochemical Principles, a Volume in Honor of Hatten S. Yoder, Jr. Spec Publ Gechem Soc, St. Louis, pp. 75–89.
Regelous, M., Niu, Y., Abouchami, W., Castillo, P.R., 2009. Shallow origin for South Atlantic Dupal Anomaly from lower continental crust: geochemical evidence from the Mid-Atlantic Ridge at 26°S. Lithos 112, 57–72.
Rehkämper, M., Hofmann, A.W., 1997. Recycled ocean crust and sediment in Indian Ocean MORB. Earth and Planetary Science Letters 147, 93–106.
Scotese, C.R., 2001. Atlas of Earth history. 2001 Paleomap Progress Report 90-0497. Department of Geology, University of Texas, Arlington, TX.
Sengör, A.M.C., Natal'in, B.A., 1996. Turkic-type orogeny and its role in the making of the continental crust. Annual Review of Earth and Planetary Sciences 24, 263.
Sengör, A.M.C., Natal'in, B.A., Burtman, V.S., 1993. Evolution of the Altaid tectonic collage and Palaeozoic crustal growth in Eurasia. Nature 364, 299–307.
Shervais, J.W., 2001. Birth, death, and resurrection: the life cycle of suprasubduction zone ophiolites. Geochemistry, Geophysics, Geosystems 2.
Shervais, J.W., Schuman, M.M.Z., Hanan, B.B., 2005. The Stonyford volcanic complex: a forearc seamount in the northern California Coast Ranges. Journal of Petrology 46, 2091–2128.
Shu, L., Wang, Y., 2003. Late Devonian–Early carboniferous radiolarian fossils from siliceous rocks of the Kelameili ophiolite, Xinjiang. Geological Review 49, 408–412.
Singer, B.S., Jicha, B.R., Leeman, W.P., Rogers, N.W., Thirlwall, M.F., Ryan, J., Nicolaysen, K.E., 2007. Along-strike trace element and isotopic variation in Aleutian Island arc basalt: subduction melts sediments and dehydrates serpentine. Journal of Geophysical Research 112, B06206.
Staudigel, H., Plank, T., White, B., Schmincke, H., 1996. Geochemical fluxes during seafloor alteration of the basaltic upper oceanic crust: DSDP Sites 417 and 418. In: Bebout, G.E., Scholl, D.W., Kirby, S.H., Platt, J.P. (Eds.), Subduction: Top to Bottom. Geophysical Monograph, 96, pp. 19–38.
Stracke, A., Bizimis, M., Salters, V.J.M., 2003. Recycling oceanic crust: quantitative constraints. Geochemistry, Geophysics, Geosystems 4, 8003.
Sun, S.S., McDonough, W.F., 1989. Chemical and isotopic systematics of oceanic basalts: implications for mantle composition and processes. Geological Society, London, Special Publications 42, 313–345.
Sun, M., Yuan, C., Xiao, W., Long, X., Xia, X., Zhao, G., Lin, S., Wu, F., Kroner, A., 2008. Zircon U–Pb and Hf isotopic study of gneissic rocks from the Chinese Altai: progressive accretionary history in the early to middle Palaeozoic. Chemical Geology 247, 352–383.
Tang, H., Su, Y., Liu, C., Hou, G., Wang, Y., 2007. SHRIMP U–Pb zircons age of plagiogranite from Karamaili ophiolite in east Junggar, Xinjiang. Geotectonica et Metallogenia 31, 110–117.
Tatsumi, Y., Kogiso, T., 2003. The subduction factory: its role in the evolution of the Earth's crust and mantle. Geological Society, London, Special Publications 219, 55–80.
Thirlwall, M.F., Smith, T.E., Graham, A.M., Theodorou, N., Hollings, P., Davidson, J.P., Arculus, R.J., 1994. High field strength element anomalies in arc lavas: source or process? Journal of Petrology 35, 819–838.
Tian, L., Castillo, P.R., Hawkins, J.W., Hilton, D.R., Hanan, B.B., Pietruszka, A.J., 2008. Major and trace element and Sr–Nd isotope signatures of lavas from the Central Lau Basin: implications for the nature and influence of subduction components in the back-arc mantle. Journal of Volcanology and Geothermal Research 178, 657–670.
Todt, W., Cliff, R., Hanser, A., Hofmann, A., 1996. ^{202}Pb–^{205}Pb double spike for lead isotopic analyses. In: Basu, A., Hart, S. (Eds.), Earth Processes: Reading the Isotopic Code, Geophysical Monograph. AGU, Washington, D. C., pp. 429–437.
Tollstrup, D., Gill, J., Kent, A., Prinkey, D., Williams, R., Tamura, Y., Ishizuka, O., 2010. Across-arc geochemical trends in the Izu–Bonin arc: contributions from the subducting slab, revisited. Geochemistry, Geophysics, Geosystems 11.
Turner, S., Hawkesworth, C., 1997. Constraints on flux rates and mantle dynamics beneath island arcs from Tonga–Kermadec lava geochemistry. Nature 389, 568–573.
Veizer, J., 1989. Strontium isotopes in seawater through time. Annual Review of Earth and Planetary Sciences 17, 141–167.
Wang, Z.H., Sun, S., Li, J.L., Hou, Q.L., Qin, K.Z., Xiao, W.J., Hao, J., 2003. Paleozoic tectonic evolution of the northern Xinjiang, China: geochemical and geochronological constraints from the ophiolites. Tectonics 22.
Wei, G.J., Liang, X.R., Li, X.H., Liu, Y., 2002. Precise measurement of Sr isotope composition of liquid and solid base using (LP) MCICPMS. Geochimica 31, 295–299.
Weis, D., Frey, F.A., 1996. Role of the Kerguelen Plume in generating the eastern Indian Ocean seafloor. Journal of Geophysical Research 101, 13831–13849.
White, W.M., 1993. $^{238}U/^{204}Pb$ in MORB and open system evolution of the depleted mantle. Earth and Planetary Science Letters 115, 211–226.
Windley, B.F., Alexeiev, D., Xiao, W., Kroner, A., Badarch, G., 2007. Tectonic models for accretion of the Central Asian Orogenic Belt. Journal of the Geological Society 164, 31–47.
Woodhead, J., Eggins, S., Gamble, J., 1993. High field strength and transition element systematics in island arc and back-arc basin basalts: evidence for multi-phase melt extraction and a depleted mantle wedge. Earth and Planetary Science Letters 114, 491–504.
Workman, R.K., Hart, S.R., 2005. Major and trace element composition of the depleted MORB mantle (DMM). Earth and Planetary Science Letters 231, 53–72.
Xiao, X., Tang, Y., Feng, Y., Zhu, B., Li, J., Zhou, M., 1992. Tectonics in Northern Xinjiang and Its Neighboring Areas.Geological Publishing House, Beijing.
Xiao, W.J., Windley, B.F., Badarch, G., Sun, S., Li, J., Qin, K., Wang, Z., 2004a. Palaeozoic accretionary and convergent tectonics of the southern Altaids: implications for the growth of Central Asia. Journal of the Geological Society 161, 339–342.
Xiao, W.J., Zhang, L., Qin, K., Sun, S., Li, J., 2004b. Paleozoic accretionary and collisional tectonics of the eastern Tianshan (China); implications for the continental growth of Central Asia. American Journal of Science 304, 370–395.
Xiao, W., Han, C., Yuan, C., Sun, M., Lin, S., Chen, H., Li, Z., Li, J., Sun, S., 2008. Middle Cambrian to Permian subduction-related accretionary orogenesis of Northern Xinjiang, NW China: implications for the tectonic evolution of central Asia. Journal of Asian Earth Sciences 32, 102–117.
Xiao, W., Windley, B., Huang, B., Han, C., Yuan, C., Chen, H., Sun, M., Sun, S., Li, J., 2009a. End-Permian to mid-Triassic termination of the accretionary processes of the southern Altaids: implications for the geodynamic evolution, Phanerozoic continental growth, and metallogeny of Central Asia. International Journal of Earth Sciences 98, 1189–1217.
Xiao, W.J., Windley, B.F., Yuan, C., Sun, M., Han, C.M., Lin, S.F., Chen, H.L., Yan, Q.R., Liu, D.Y., Qin, K.Z., Li, J.L., Sun, S., 2009b. Paleozoic multiple subduction–accretion processes of the southern Altaids. American Journal of Science 309, 221–270.
Xiao, W., Huang, B., Han, C., Sun, S., Li, J., 2010. A review of the western part of the Altaids: a key to understanding the architecture of accretionary orogens. Gondwana Research 18, 253–273.
Xu, J.-F., Castillo, P.R., 2004. Geochemical and Nd–Pb isotopic characteristics of the Tethyan asthenosphere: implications for the origin of the Indian Ocean mantle domain. Tectonophysics 393, 9–27.
Xu, J.-F., Castillo, P.R., Li, X.-H., Yu, X.-Y., Zhang, B.-R., Han, Y.-W., 2002. MORB-type rocks from the Paleo-Tethyan Mian–Lueyang northern ophiolite in the Qinling Mountains, central China: implications for the source of the low $^{206}Pb/^{204}Pb$ and high $^{143}Nd/^{144}Nd$ mantle component in the Indian Ocean. Earth and Planetary Science Letters 198, 323–337.
Xu, X., He, G., Li, H., Ding, T., Liu, X., Mei, S., 2006. Basic characteristics of the Karamay ophiolitic me1ange, Xinjiang, and its zircon SHRIMP P dating. Geology in China 33, 470–475.
Zhang, C., Huang, X., 1992. The ages and tectonic settings of ophiolites in west Junggar, Xinjiang. Geological Review 36, 509–524.
Zhang, S.Q., Mahoney, J.J., Mo, X.X., Ghazi, A.M., Milani, L., Crawford, A.J., Guo, T.Y., Zhao, Z.D., 2005. Evidence for a widespread Tethyan Upper Mantle with Indian-Ocean-type isotopic characteristics. Journal of Petrology 46, 829–858.
Zhang, Z.C., Zhou, G., Kusky, T.M., Yan, S.H., Chen, B.L., Zhao, L., 2009. Late Paleozoic volcanic record of the Eastern Junggar terrane, Xinjiang, Northwestern China: major and trace element characteristics, Sr–Nd isotopic systematics and implications for tectonic evolution. Gondwana Research 16, 201–215.
Zhang, J.E., Xiao, W., Han, C., Mao, Q., Ao, S., Guo, Q., Ma, C., 2011. A Devonian to Carboniferous intra-oceanic subduction system in Western Junggar, NW China. Lithos 125, 592–606.
Zheng, J., Sun, M., Zhao, G., Robinson, P.T., Wang, F., 2007. Elemental and Sr–Nd–Pb isotopic geochemistry of Late Paleozoic volcanic rocks beneath the Junggar basin, NW China: implications for the formation and evolution of the basin basement. Journal of Asian Earth Sciences 29, 778–794.